COPY 1

PM 84/29

DOT/FAA/PM-84/29

Program Engineering
and Maintenance Service
Washington, D.C. 20591

FAA WJH Technical Center
00092761

Microburst Wind Structure and Evaluation of Doppler Radar for Wind Shear Detection

James W. Wilson
Cathy Kessinger
Rita D. Roberts
John McCarthy

Joint Airport Weather Studies Project
National Center for Atmospheric Research
Boulder, Colorado 80307

DEC 3 1984
FAA WJH TECH. CENTER LIBRARY
ATLANTIC CITY, N.J. 08405

October 1984

Final Report

FAA WJH Technical Center
Tech Center Library
Atlantic City, NJ 08405

AVAILABLE IN
ELECTRONIC FORMAT

This Document is available to the public through the National Technical Information Service, Springfield, Virginia 22161.

U.S. Department of Transportation
Federal Aviation Administration

NOTICE

This document is disseminated under the sponsorship of the Department of Transportation in the interest of information exchange. The United States Government assumes no liability for its contents or use thereof.

Technical Report Documentation Page

1. Report No.	2. Government Accession No.	3. Recipient's Catalog No.
DOT/FAA/PM-84/29		

4. Title and Subtitle	5. Report Date
Microburst Wind Structure and Evaluation of Doppler Radar for Airport Wind Shear Detection	October 1984
	6. Performing Organization Code
7. Author(s) James W. Wilson, Rita D. Roberts, Cathy Kessinger, John McCarthy	8. Performing Organization Report No.
9. Performing Organization Name and Address Joint Airport Weather Studies Project National Center for Atmospheric Research P. O. Box 3000 Boulder, Colorado 80307	10. Work Unit No. (TRAIS)
	11. Contract or Grant No. DTFA01-82-Y-10513
12. Sponsoring Agency Name and Address Department of Transportation Federal Aviation Administration Program Engineering and Maintenance Service Washington, D.C. 20591	13. Type of Report and Period Covered Final Report
	14. Sponsoring Agency Code APM-310

15. Supplementary Notes

Research performed under Interagency Agreement No. DTFA01-82-Y10513 between the National Science Foundation and the Department of Transportation, Federal Aviation Administration.

16. Abstract

Doppler weather radar data from the Joint Airport Weather Studies (JAWS) Project are used to determine the horizontal and vertical structure of airflow within microbursts. Typically, the associated downdraft is about 1 km wide and begins to spread horziontally at a height below 1 km. The median time is 5 min from initial divergence at the surface to maximum differential wind velocity across the microburst. The height of maximum differential velocity is 75 m. The median velocity differential is 22 m/s over an average distance of 3.1 km. The outflow is assymetric, averaging twice as strong along the maximum shear axis compared to the minimum axis.

Doppler radar could be an effective means for identifying microbursts and warning aircraft of wind shear hazards. For microburst detection such a radar must be able to measure wind velocities in clear air as well as heavy rain and hail. Scan update rates should be approximately every 2 min and the lowest few hundred meters of the atmosphere must be observed. Ground clutter must be considerably reduced from levels typically obtained with present Doppler radars. New antenna technology and signal processing techniques may solve this problem. Automated range and velocity unfolding is required, as well as automated identification and dissemination techniques.

17. Key Words	18. Distribution Statement
Aviation Safety, Doppler Radar, Joint Airport Weather Studies, Microbursts, Wind Shear Detection, Weather Radar	Document is available to the public through the National Technical Information Service, Springfield, Virginia, 22161.

19. Security Classif. (of this report)	20. Security Classif. (of this page)	21. No. of Pages	22. Price
Unclassified	Unclassified	43	

Form DOT F 1700.7 (8-72) Reproduction of completed page authorized

TABLE OF CONTENTS

	Page
1. INTRODUCTION	1
2. DATA	2
3. MICROBURST OBSERVATIONS	5
a. Flow Fields	5
b. Intensity and Evolution	9
c. Forecasting	13
d. Summary of Microburst Structure and Evolution	17
4. PROPOSED DOPPLER DEPLOYMENTS	19
a. Dual-Doppler	20
b. Single-Doppler, Off-Airport	20
c. Single-Doppler, On-Airport	22
d. Radar Characteristics	
5. CONCLUSIONS AND RECOMMENDATIONS	27
6. ACKNOWLEDGMENTS	29
7. REFERENCES	29
APPENDIX A	A1
APPENDIX B	B1

LIST OF FIGURES

		Page
Figure 1.	Map illustrating JAWS Project facilities situated in the vicinity of Denver's Stapleton International Airport.	3
Figure 2.	Time evolution (1641-1648 MDT) of the horizontal velocity field (ground relative) for a microburst on 14 July 1982. Winds are based on a dual-Doppler analysis for a height of ∿50 m AGL. Contours are radar reflectivity factor (dBZ_e). Wind speed is given by the scale vector at figure top.	6
Figure 3.	Time evolution (1447-1452) of the horizontal and vertical velocity fields within a microburst on 14 July 1982. (a) and (d) Horizontal eddy wind (mean wind subtracted) and reflectivity at 50-100 m AGL at 1447 and 1452, respectively. (b) and (e) Vertical cross section of winds along line A-B at 1447 and 1452 respectively. (c) and (f) Vertical cross section of winds along line C-D at 1447 and 1452, respectively. The figure legends a-f are in the upper right corner of each panel.	8
Figure 4.	High resolution vertical profiles of the radial wind differential across three microbursts. The data are single Doppler observations at close range (4-10 km). The average curve is for six cases between 8 and 26 km.	10
Figure 5.	Doppler observed maximum low-altitude velocity differentials (ΔV_r) associated with microbursts versus the radar reflectivity at a height of 500 m.	11
Figure 6.	Percent of microbursts reaching maximum velocity differential as a function of the time from initial divergence.	14
Figure 7.	Vertical cross section of the evolution of the microburst wind field based on a summary of data in Section 3. T is the time of initial divergence at the surface. The shading refers to the vector wind speeds.	18
Figure 8.	Locations of three proposed Doppler radar systems for detecting low-level wind shear near an airport. The airport is centered within the 10 km range ring. The radars labeled [a] represent a dual-Doppler system, the stippled area represents the area where accurate dual-Doppler winds can be obtained, [b] a single-Doppler off-airport system, and [c] a single-Doppler on-airport system.	21

Page

Figure 9. Simulation of the radial velocity field observed by two hypothetical off-airport radars viewing a microburst at 1846 MDT on 5 August 1982. (a) Actual horizontal windfield at a height of 50-80 m based on a dual-Doppler analysis. A hypothetical runway of 2.7 km is superimposed on the microburst. The contours represent radar reflectivity factors (dBZ_e). (b) Simulated Doppler radial winds for a radar located 13 km southeast of the microburst. (c) same as (b) except for a radar located 13 km northeast of the microburst. 23

Figure 10. Comparison of ground clutter reflectivity patterns from collocated and matched beam 10 cm and 3 cm radars. Range marks are at 10 km intervals and the reflectivity scale is given by the bar at the bottom. The data are from the CP-2 radar scanning at an elevation angle of 0.5°. 25

LIST OF TABLES

Table 1. Asymmetry of low-altitude wind shear for 13 microbursts at various lengths. 15

Table 2. Time and space scales of microburst velocity differentials (ΔV_r) from the time of initial Doppler-observed, low-level divergence to maximum ΔV_r. The maximum reflectivity at 500 m within each microburst cell is also given. 16

MICROBURST WIND STRUCTURE AND EVALUATION OF DOPPLER RADAR FOR AIRPORT WIND SHEAR DETECTION

James W. Wilson, Rita D. Roberts, Cathy Kessinger, and John McCarthy

National Center for Atmospheric Research[1]
Boulder, Colorado 80307

1. INTRODUCTION

Wind shears in the lowest few hundred meters of the atmosphere have been responsible for a number of aircraft accidents (Fujita, 1980). McCarthy et al. (1980) proposed that a Doppler radar could be used to detect and warn of wind shears in the airport vicinity. Wilson et al. (1980) showed that wind shear phenomena exist on spatial scales critical to aircraft performance and that a Doppler radar could provide important headwind-tailwind information along a flight path. Mahapatra et al. (1982) considered several systems for detecting a variety of wind-shear-producing phenomena and concluded that a warning system could be developed using Doppler radar.

Significant shears can be produced by low-altitude jets, fronts, gust fronts, gravity waves, topography, and convective storms. We feel that small-scale, near surface, divergent outflows from convective storms are the most hazardous to aircraft and most difficult to detect. This is because of their small scale, short lifetime and strongly divergent nature. An aircraft penetrating such a phenomenon on either approach-to-landing or takeoff will lose airspeed, a particularly dangerous situation near the ground.

Fujita (1981) gave the name "microburst"[2] to a downdraft that induces a sudden outflow of damaging horizontal winds at the surface with a horizontal extent between 0.4 and 4.0 km. This is the scale of phenomena we feel is most dangerous to aircraft and is the primary focus of this paper. Outflows on this scale can be inferred from the early work of Byers and Braham (1949). During the Northern Illinois Meteorological Research on Downbursts (NIMROD), the first measurements of airflow within microbursts were obtained with Doppler radar (Fujita, 1981). Because of the 60 km spacing of the radars during NIMROD, only single Doppler analyses were possible. It then became the objective of the Joint Airport Weather Studies (JAWS) Project (McCarthy et al., 1982) to design a suitable Doppler radar network for observing the three-dimensional wind field within a microburst.

---

[1]The National Center for Atmospheric Research is sponsored by the National Science Foundation.

[2]In this study the definition of a microburst is modified to refer to Doppler radar observed diverging outflows near the surface associated with convective storms. The differential Doppler velocity across the divergence center must be >10 m s^{-1} and the initial distance between maximum approaching and receding centers must be ≤ 4 km.

Utilizing the JAWS data, we characterize the wind structure of microbursts and then examine the utility of various ground-based, microwave, and pulsed Doppler radar alternatives for detection and warning of low-altitude wind shear in the approach-departure vicinity of an airport. Other techniques for detecting wind shear such as Doppler lidars, FM-CW radars, acoustic sounders, and anemometer arrays are not discussed. The applicability ofthese devices for wind shear detection is discussed in a recent National Academy of Science report (National Research Council, 1983). The physical mechanisms which drive the downdrafts and the likelihood that the wind structures observed in the Denver area may occur in other regions are beyond the scope of this paper.

In Section 3, microburst features are examined so that the necessary Doppler radar characteristics can be specified. For example, the microburst depth of outflow, horizontal scale, flow characteristics, time evolution, and reflectivity are needed to establish radar resolution, scanning strategies, and sensitivity. In Section 4, three proposed radar systems for measuring low-altitude wind shear are examined. In evaluating these proposed systems, wind information that is important to aircraft performance will be considered.

2. DATA

Doppler data used in this paper are from the NCAR Doppler radars [CP-2 (10 cm), CP-3 (5 cm) and CP-4 (5 cm)]. The radars were located in a small triangle (14, 18 and 28 km lengths of sides) with the southernmost radar located at the center of Stapleton International Airport in Denver, Colorado (see Fig. 1). These research radars have 1°, half-power beam widths. CP-2 has a minimum detectable signal of $\sim$-18 dBZ_e at 25 km, and CP-3 and CP-4, -5 dBZ_e at 25 km. These radars have excellent warm season, boundary layer, optically clear air detection capabilities. CP-2 routinely observes reliable velocities throughout the boundary layer to a range of at least 100 km; the corresponding range for CP-3 and CP-4 is 50 km. However, both main beam and sidelobe ground clutter contamination can limit low-altitude wind observations.

We have identified and examined in varying degrees of detail $\sim$70 microbursts in the JAWS Doppler radar data set which spanned the time from 15 May to 13 August 1982. The detection of a microburst was based on at least one Doppler radar observing a diverging Doppler velocity signature. At initial divergence, the distance from the maximum approaching to the maximum receding cores must be $\leq$ 4 km and the velocity differential $>$ 10 m/s. Undoubtedly more events occurred since all the data have not been examined and the radars were not scanning all the time in all directions. Also, there may have been some very small-scale (<1 km) events associated with virga that went undetected, at least by radar.

Doppler-derived wind fields for 13 cases are obtained with an overdetermined dual-Doppler synthesis program developed at the National Severe Storms Laboratory (Kessinger et al., 1983). Data editing is performed on NCAR's Research Data Support System (RDSS) which is an imaging, interactive computer system (Oye and Carbone, 1981). The vertical wind component is derived from an upward integration of the anelastic mass continuity equation. A lower boundary condition of zero vertical velocity is assumed. To

incompressible?

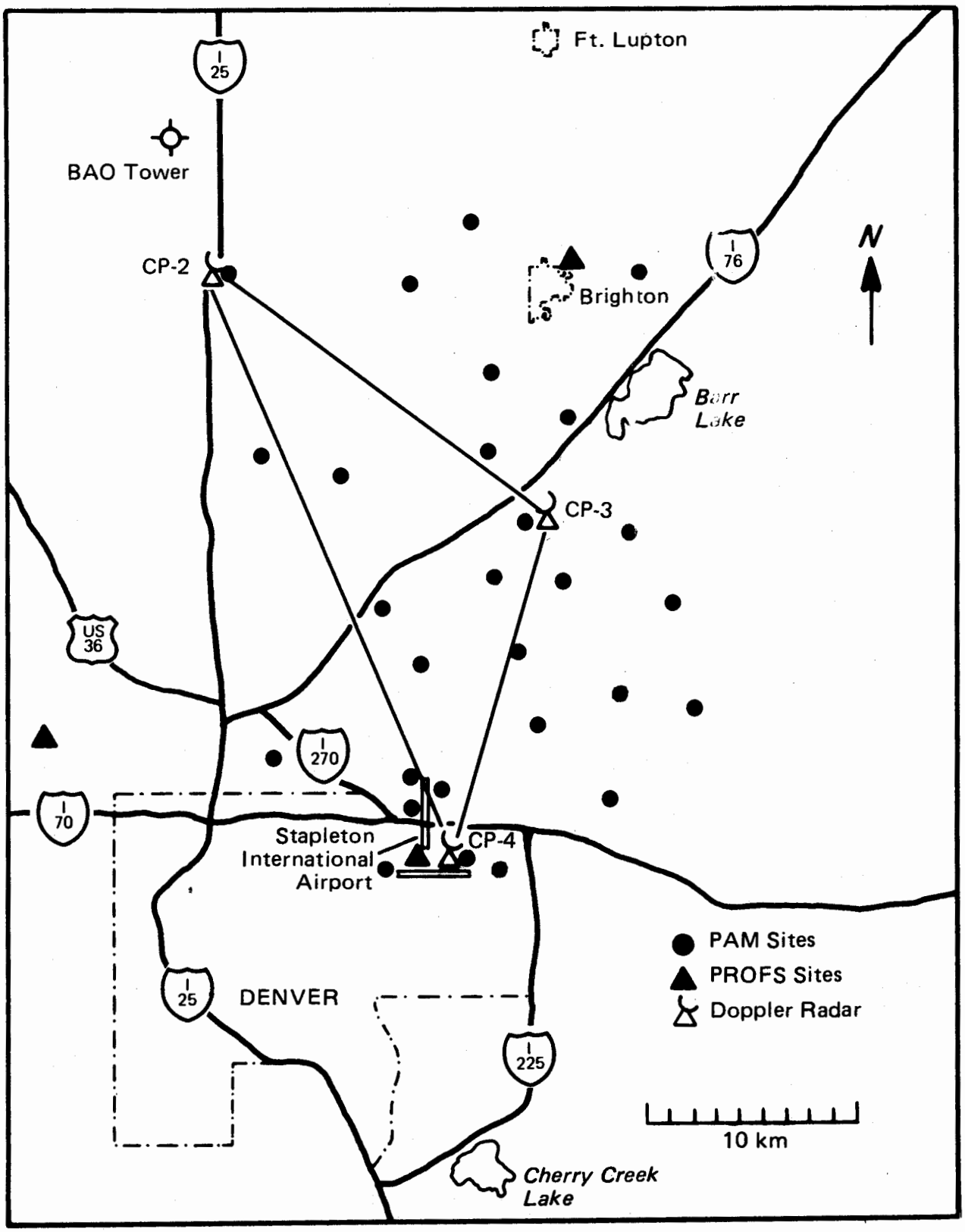

Figure 1. Map illustrating JAWS Project facilities situated in the vicinity of Denver's Stapleton International Airport.

optimize the resolution and accuracy of the three-dimensional wind analyses, the radars were closely located and data were collected as close to the ground as possible. Generally, the lowest-observed radar level was centered 25-150 m above the ground. Data density in elevation and azimith was usually <0.5° and <0.8°, respectively. The radial length of the received pulse volume was 150 m. Only microbursts within 30 km of the radars were studied. The average microburst distance was 17 km. The combination of close radar spacing and short distance to the microbursts made it possible to generate wind analysis of high resolution near the ground.

The need for data close to the ground resulted in extensive use of data collected with an elevation angle near 0.0°. For these angles much of the radiation in the lower half of the beam was disrupted or eliminated by intervening ground targets. Also the radar beam has a finite dimension which smooths the wind pattern. The smoothing is dependent on radar range, beam pattern and reflectivity distribution over the beam. Because of these effects and atmosphere-induced propagation anomalies, it is nearly impossible to know the actual height of the effective beam center and the degree of spatial smoothing. For this paper, it is assumed the effective beam height is 0.2° for a 0.0° elevation angle and that the measured wind is representative of the actual wind at this height.This is based on a graphical analysis that utilized only the top half of the beam radiation pattern.

Generally, it was possible to obtain wind vectors on a grid with a horizontal and vertical spacing of 150-250 m. The interpolation scheme used an influence radius equal to the grid spacing. Because of over sampling, the grid interval was typically less than the pulse volume defined by the 1° half power beam width (∿300 m in the horizontal and vertical). We estimate that wind features with scales greater than 1 km (scale defined as 1/2 wavelength) are well resolved, and considerable information is obtained on scales down to 600 m. Wind features with scales of 1-4 km are most critical to aircraft performance (McCarthy and Norviel, 1982); therefore, the most important scale features are adequately resolved.

Numerous errors can affect the accuracy of the Doppler-derived wind fields. With one exception, only low-altitude, horizontal wind fields are used for this paper. Important error sources for these wind fields are: statistical uncertainties in the radial velocity estimates (Doviak et al., 1976), geometrical considerations (Ray et al., 1979; and Miller and Strauch, 1974), non-simultaneity of the observations (Miller and Kropfli, 1980) and contamination of the radial velocity estimate by ground clutter. An error analysis detailed in Appendix A shows that for cases presented in this paper, the first two errors combine to give, as an upper limit, a 1-2 m/s error in derived horizontal winds. The third error is negligible since the radars started scanning the same area within seconds of each other and only required a few seconds to complete each scan. The fourth error source (clutter contamination) is potentially the most serious. This how? error was controlled by careful editing of the data to remove all radial velocities believed to be clutter contaminated. Appendix B discusses this data editing technique. Also the NCAR radar processors have the characteristic that when the Doppler velocity spectra are bimodal (one spectrum near

zero associated with ground return and another offset from zero associated with meteorological return) they capture ("capturing effect") the velocity of the strongest mode, especially for signals greater than -95 dBm (Frush, 1981). Thus, the reported radial velocity is either close to zero corresponding to the clutter or close to the velocity of the meteorological signal without significant bias toward zero, provided the meteorological signal strength exceeds the clutter signal strength by more than ∿3 dB. From the errors discussed above, it is likely that the horizontal velocities are accurate to within 2 m/s.

Errors in vertical velocity are potentially larger than those for horizontal velocities. For the case described later, 2.5 min was required to scan the storm volume. Thus, error sources from evolution and advection may be important (Carbone, 1981; and Ray et al., 1980). Fortunately, horizontal advection was negligible. However, evolutionary effects are unknown. The error occurs in assuming the horizontal winds, at each height, are constant for up to half the volume scanning period (90 s). For microbursts, the horizontal winds near the surface may show significant changes within 90 s. The primary effect is to alter the magnitude of the vertical motions rather than the overall wind structure.

The divergence in a microburst decreases rapidly from roughly 200 m to 1 km in altitude. Accurate measurements of divergence in the lowest 1 km are essential if vertical motions are to be obtained by vertical integration of the mass continuity equation. This was accomplished by taking great care to obtain accurate horizontal wind fields at 150 m intervals starting at about 75 m. The analyses assume the divergence at the surface is equal to that at the lowest observed level (∿75 m in this case) and the vertical velocity at the surface is zero. As will be discussed later, we believe this to be a good assumption except for possibly the lowest few meters.

While the effect of clutter biasing of the velocities or failure to remove clutter would result in underestimates of the divergence, we feel confident that the editing technique and the Doppler processor "capturing effect" have reduced this problem to minor importance for the analysis presented. While estimation of the total error in the vertical velocity is difficult, we believe the primary error sources are statistical uncertainties in radial velocity, uncertainties in mean reflectivity weighted raindrop fall speeds, error in the surface boundary condition, evolutionary change during the scan period, and upward integration of the mass continuity equation. Computations based on these error sources suggest the errors are probably less than 0.5 m/s at 100 m increasing to 2 m/s at 1400 m.

3. MICROBURST OBSERVATIONS

a. Flow Fields

Figure 2 shows the time evolution of the horizontal winds of a microburst on 14 July 1982. These analyses were based on data from three Doppler radars using the overdetermined dual-Doppler analysis technique mentioned above. The plots are for a height of ∿50 m AGL (the grid spacing is 250 m and there is 2.5 min between analyses). The contours are equivalent radar reflectivity factor (dBZ_e). At 1641:15 MDT the first sign of

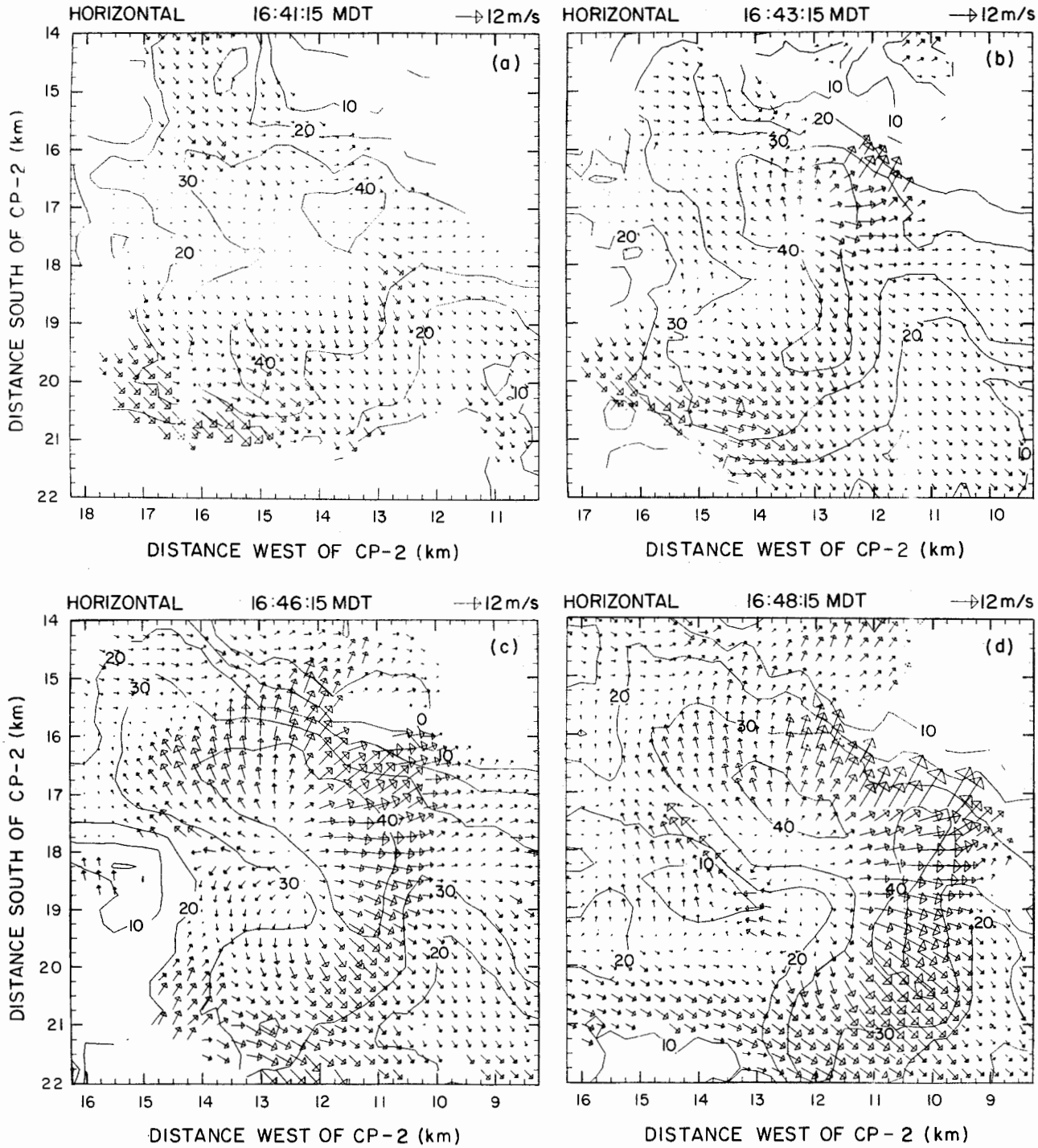

Figure 2. Time evolution (1641-1648 MDT) of the horizontal velocity field (ground relative) for a microburst on 14 July 1982. Winds are based on a dual-Doppler analysis for a height of ∿50 m AGL. Contours are radar reflectivity factor (dBZ_e). Wind speed is given by the scale vector at figure top.

divergent outflow appears at the south end of the 40 dBZ_e contour (13.5 W, 17.5 S relative to CP-2). The divergence is 5 x 10^{-3} s^{-1} and winds are less than 6 m/s. Two minutes later, the divergence has increased to 20 x 10^{-3} s^{-1} and the maximum wind speed to 12 m/s. By 1646:15 and 1648:15 the area of divergence has increased substantially and maximum winds have increased to at least 20 m/s. By 1652 (not shown), 4 min after Fig. 2d, the divergent flow became disorganized and maximum speeds are less than 10 m/s. The size, strength and evolution of this microburst is typical of other microbursts observed during JAWS.

Figure 3 is an example of both the horizontal and vertical airflow in a microburst on the same day as Fig. 2. Sufficient data were available for only two analyses 5 min apart. Data density in the vertical was very high (elevation angle separation 0.2° to 0.3°). The horizontal velocity fields shown are for a height of 50-150 m. At 1447 (Fig. 3a), the surface divergence (15 x 10^{-3} s^{-1}) near 13.9 E, 1.4 S has developed in the past 2 min. By 1452 (Fig. 3d) the center of the divergence has moved south 2-3 km and has spread from a small center into a line about 3 km long with maximum divergence of 25 x 10^{-3} s^{-1}. While the surface divergent center moves southward, it does not appear to be a horizontally advective phenomena because reflectivity features show no motion. Rather, a north-south line of downdraft gives an apparent southward motion by reaching the surface first to the north and progressing with time southward.

Two cross sections are shown for each time period. Cross section A-B is through the divergence center at 1452. Figure 3e shows the downdraft, which has a diameter of 1 km, beginning to spread horizontally at a height of ~600 m. The downdraft speed is 12 m/s at a height of 1200 to 600 m and decreases to 9 m/s and 6 m/s at 400 m and 200 m, respectively. The horizontal vortex flow at the east and west edges of the microburst is a common feature observed in other JAWS microbursts for which similar cross sections are available. Other investigators have observed similar flows with both gust fronts and microbursts (Charba, 1974; Wakimoto, 1982; Fujita 1981; Mueller and Hildebrand, 1983). The 1447 cross section (Fig. 3b) shows the downdraft has not penetrated below 1 km. Since a downdraft of 10 m/s could move 3 km vertically in 5 min, it is not surprising that such a dramatic change occurred in cross section A-B in 5 min.

Cross section C-D at 1447 (Fig. 3c) shows a microburst in mid-air. Horizontal divergence and horizontal roll vortices have developed while the downdraft is still 600 m above the surface. Fujita and Wakimoto (1983) hypothesize a similar structure for the airflow prior to contact with the surface. The C-D cross section for 1452 (Fig. 3f) shows the downdraft has reached the ground. The diameter of the downdraft has increased from 1.5 km to 3.5 km and the maximum speed from 6 to 10 m/s.

Considering the many potential errors in a dual-Doppler analysis, particularly in the vertical motions, the question arises as to the accuracy of the remarkable detail shown in Fig. 3. There are several factors which give credence to the results. First, similar four-dimensional analyses have been performed for three additonal microbursts and they all exhibit the same general features. Second, there is reasonable time continuity in the wind structure from one analysis to the next. Third, in a study by Mueller and Hildebrand (1983) for a JAWS microburst, they compared

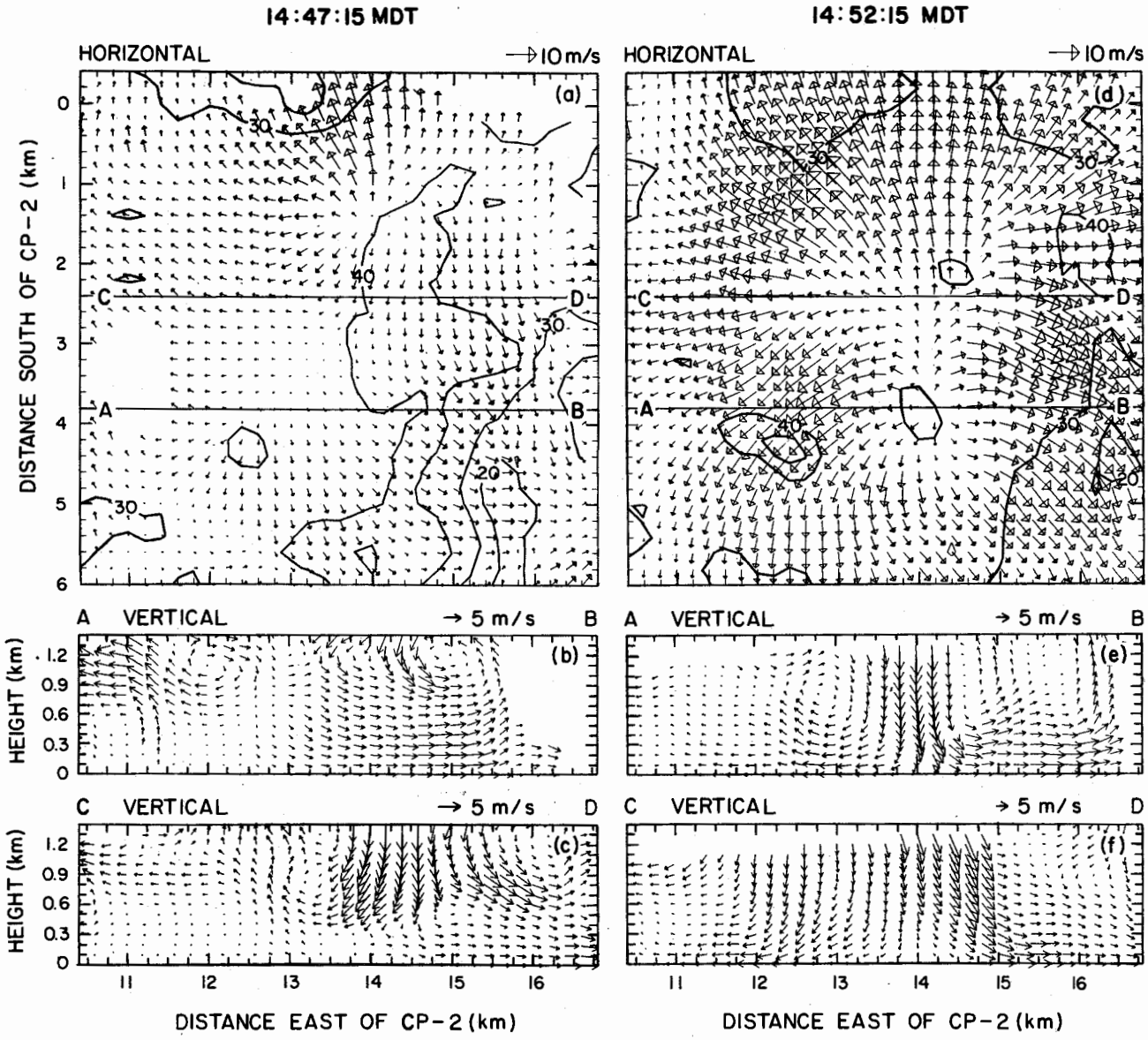

Figure 3. Time evolution (1447-1452) of the horizontal and vertical velocity fields within a microburst on 14 July 1982. (a) and (d) Horizontal eddy wind (mean wind subtracted) and reflectivity at 50-100 m AGL at 1447 and 1452, respectively. (b) and (e) Vertical cross section of winds along line A-B at 1447 and 1452, respectively. (c) and (f) Vertical cross section of winds along line C-D at 1447 and 1452, respectively. The figure legends a-f are in the upper right corner of each panel.

vertical motion profiles from a ground-based dual-Doppler analysis with those measured by an airborne Doppler radar flying over the microburst center. Their results show these two independent techniques gave very similar vertical velocity profiles. Their study used the same ground-based radars, editing techniques, and analysis programs as in this study.

Examination of the divergence or differential wind velocities within the microburst in Fig. 3 shows maximum values are in the lowest 200 m. This is in agreement with a Doppler analysis of an Illinois microburst by Fujita (1981). To examine further the height (AGL) of the maximum differential velocity, vertical profiles from single Doppler radar are shown in Fig. 4 for three microbursts. The differential velocity refers to the difference between the maximum receding and maximum approaching radial velocities. These cases were selected for presentation since the microbursts were close to the radar (4-10 km) and data spacing in the vertical was <100 m while still maintaining considerable independence between samples (elevation steps 0.7-1.0°). All three profiles have essentially the same shape; the peak differential is near 75 m (AGL) with a very gradual decrease above and below. It is possible that the decrease in wind speeds below 75 m is an artifact from clutter contamination of the velocities; however, we believe it is largely the result of surface frictional slowing of the real wind. Comparison of anemometer winds at 3 m height with Doppler-derived, low-level winds for three JAWS microbursts show the anemometer winds are typically smaller (Kessinger et al., 1983); this was attributed to frictional slowing of the wind. An average profile at the time of maximum velocity differential for six cases is also shown in Fig. 4. The data for these cases had a similar vertical spacing, but because of slightly greater radar range (8-26 km), the data are likely less independent and the profiles are smoother. Vertical profiles 2.5 min and 5 min before and after the time of maximum differential are similar in shape. The similarity in the shape of all profiles is striking, suggesting they are representative of the general microburst population.

The vertical cross sections in Fig. 3e showed the microburst diverging outflow was below 1 km. The representativeness of this observation was confirmed by examining 56 microbursts where there were sufficient data to identify the top of the diverging outflow by at least one Doppler radar. For 90% of these cases, the top of the divergent flow was between 300 and 1200 m.

This finding shows the necessity to observe the lowest 1 km of the atmosphere. While not pertinent to this paper, traditional multiple Doppler analyses on the storm scale typically do not observe the divergence below ∿1 km and assume the vertical velocity at that level is zero. We wonder, even for this larger scale, if this assumption does not produce large errors in vertical velocity.

b. Intensity and Evolution

Figure 5 shows the maximum differential radial velocity (ΔV_r) observed near the surface for each of 68 microbursts versus the maximum reflectivity observed at 500 m AGL from the cell producing the microburst. In practice a cell was loosely defined as a closed reflectivity contour at least 2 km in diameter. The maximum ΔV_r varies from 10-48 m s^{-1}. The median value is

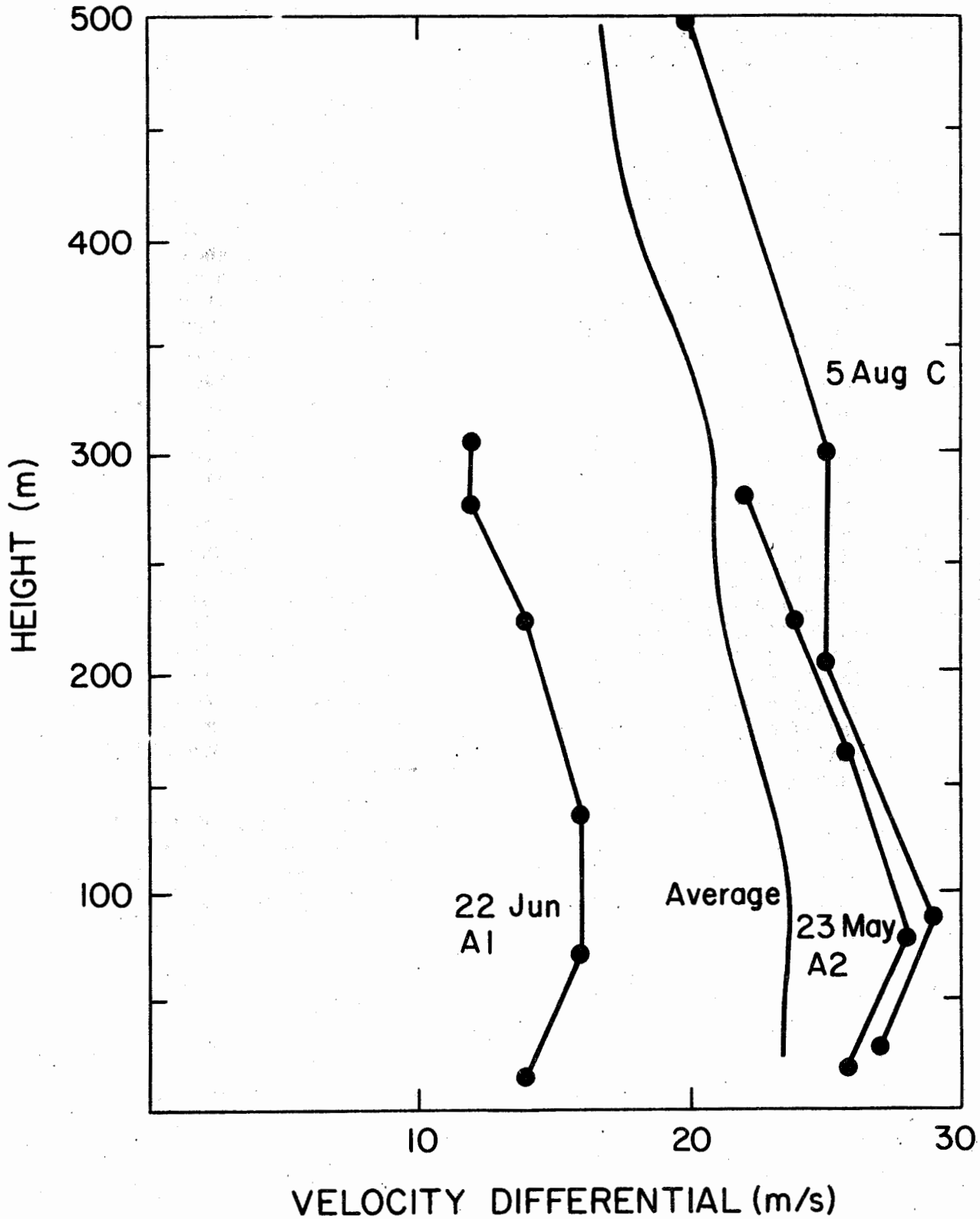

Figure 4. High resolution vertical profiles of the radial wind differential across three microbursts. The data are single Doppler observations at close range (4-10 km). The average curve is for six cases between 8 and 26 km.

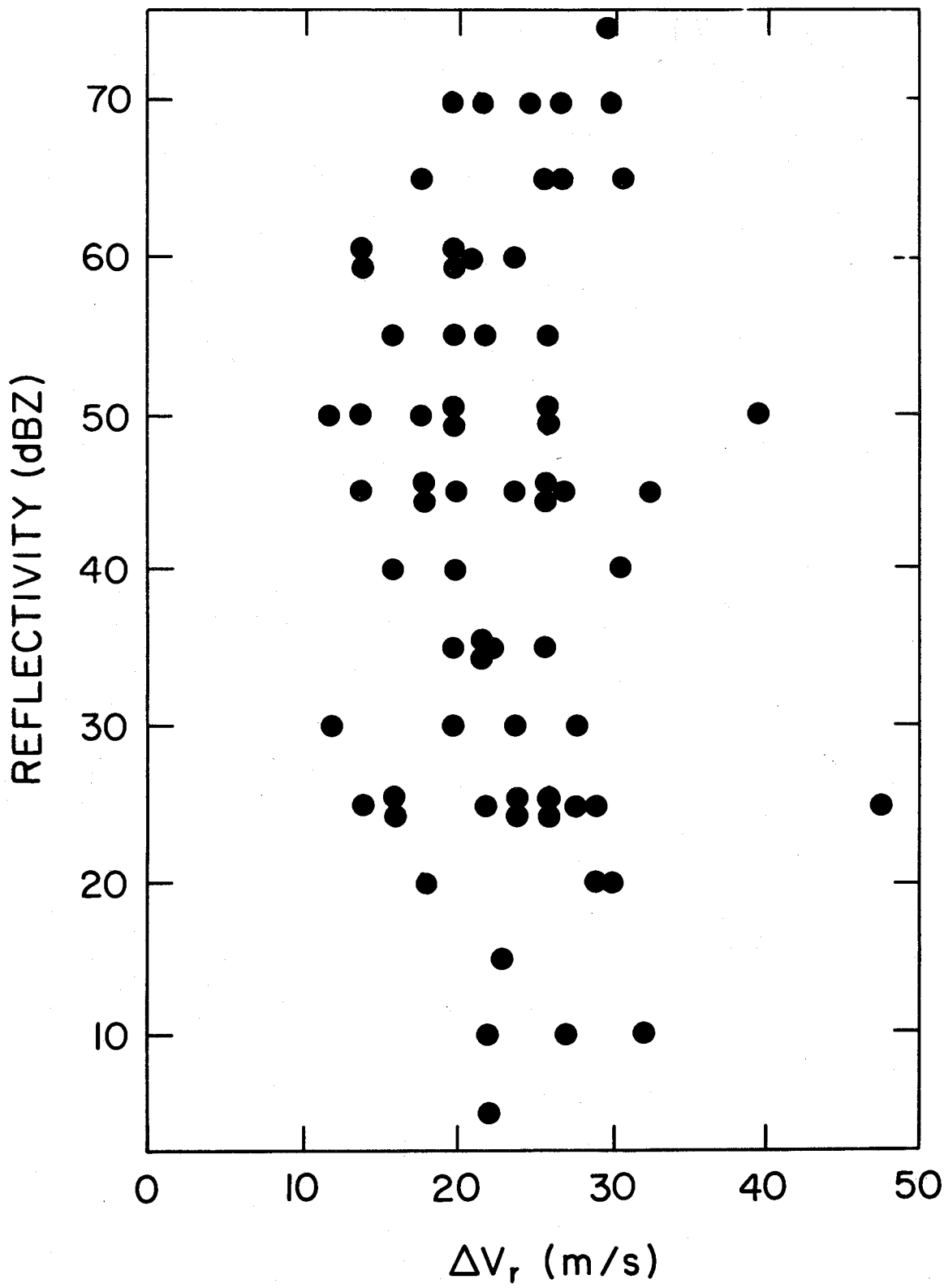

Figure 5. Doppler observed maximum low-altitude velocity differentials (ΔV_r) associated with microbursts versus the radar reflectivity at a height of 500 m.

22 m/s, essentially the same headwind-tailwind differential that Fujita (1983) and Caracena et al. (1983) reported for the Pan American airline crash at Kenner, Louisiana, in 1982. In this case, a microburst was cited as the probable cause (NTSB, 1983). If these findings are accurate, potentially lethal microbursts are common, at least in the Denver area. From Fig. 5 it is obvious that no relationship exists between storm reflectivity and microburst strength. Thus, even though a shower is weak, it may produce a dangerous microburst. The strongest case observed occurred with a 25 dBZ_e echo. For any individual microburst, the divergence center was nearly always coincident with the reflectivity maximum. This is clearly evident in Figs. 2 and 3. Figure 5 also shows microbursts were associated with storms having reflectivities at 500 m AGL between 10 and 75 dBZ_e. In several of the cases studied, the reflectivity was <10 dBZ_e below 500 m, the lowest being -5 dBZ_e. Thus, for a number of microbursts few or no raindrops reached the ground. The occurrence of dry microbursts--those with little or no rain at the surface--are likely confined primarily to the western states where deep, dry boundary layers are prevalent. In these cases, evaporational cooling of the air by falling rain is probably instrumental in forcing the downdraft. The wet microburst was also common in the data set, and while other mechanisms are likely responsible for forcing these downdrafts, there were no obvious differences in their outflow structure. However, definitive studies have yet to be completed.

In Fig. 5 the differential velocity is taken from the radar that reported the maximum differential. If the outflow is not symmetrical, the radar-measured differential velocity could vary considerably with changes in the viewing angle. For each microburst in Fig. 5, the measured differential velocity from each radar was compared. For 92% of the cases, all radars scanning the area observed a diverging microburst-type signature. This excludes several cases where blockage or clutter obscured the event. The differential velocities measured by the different radars (excluding the nondetection cases) had a 0.76 coefficient of correlation, indicating that modest symmetry existed.

The symmetry of the horizontal flow within microbursts is important when considering the radar siting question. For this reason, the symmetries of outflows from 13 microbursts were examined in detail. These cases were selected as representing a variety of microburst types of high data quality located in a good dual-Doppler analysis area. They are likely representative of the outflow asymmetry in the general microburst population. For each case, a near-surface (height 0-125 m) horizontal wind field was obtained from a dual-Doppler analysis. The horizontal wind analyses are considered to be highly accurate since all microbursts were within 25 km of the radars and the radar viewing angles differed by more than 40°. Utilizing the synthesized wind fields, the wind components along 12 diagonals passing through the center of each microburst were measured, simulating Doppler radial wind components at 15° intervals. From these data, the maximum shear ($\Delta V/\Delta R$) along each diagonal was determined for lengths (ΔR) of 0.6, 1.0, 2.0, 3.0 and 4.0 km. The results are shown in Table 1. From the shear columns in Table 1, the maximum differential velocities occur at the greater distances (3 and 4 km), even though the

actual shear magnitude is greatest over the shortest distance (600 m).[3] Thus, ΔV increases at a slower rate than ΔR. Examination of the asymmetry columns show that on the average the minimum shear is less than half of that along the maximum shear axis. The asymmetry also increases with increasing length. In the worst case the minimum shear is only 15% to 20% of the maximum. Thus, considerable error can occur in estimating the shear magnitude along any path that is not parallel to the beam.

For the cases in Table 1, the orientation of the maximum shear axes varied from 10° through 170° (i.e., essentially every direction except directly north-south). While 8 of the 13 cases were within 15° of east-west, 4 of these were associated with the same day (5 Aug). While the data sample is small, it does not appear there is a preferred orientation of the maximum shear axis. It is also unknown how the shear axis may compare with the storm's direction of motion.

From Figs. 2 and 3, the microburst flow features are seen to evolve rapidly. Table 2 provides information on the time and space scale of microbursts. The only cases listed are those with low-altitude radar scans at least every 2.5 min with data beginning prior to the microburst onset. The magnitude of the differential velocity and distance between the maximum approaching and receding velocities are recorded at both the time the divergent outflow first became apparent and when the differential velocity reached a maximum. The time from first divergence until maximum ΔV_r ranged between 0 and 28 min; the median was 5 min. The data in Table 2 on the time to reach maximum ΔV_r have been plotted in Fig. 6. Only 3 of 38 microbursts were at maximum ΔV_r at the initial observation of divergence, 53% reached maximum before 5 min, and 95% before 10 min. The average initial ΔR and ΔV_r were 1.8 km and 12 ms^{-1}, respectively. At the time of maximum ΔV_r, the average ΔR and ΔV_r values increased to 3.1 km and 24 m s^{-1}, respectively. Once ΔV_r reaches a maximum, it frequently decreases rapidly, at times almost completely dissipating within 5 min. On other occasions, it may grow in scale to become a long-lasting divergent area or line.

c. Forecasting

Specific forecasts of microburst location and intensity are desired even if only a few minutes of advance warning are possible. Because the microburst upon reaching the surface typically takes ∿5 min to reach maximum intensity (Fig. 6), some advanced warning exists prior to the most hazardous conditions. The most hazardous condition for aircraft is when the shear over a distance of approximately 3 km reaches a maximum. Little additional advanced warning can be obtained by looking for divergence aloft since it doesn't begin until the downdraft is less than 1 km above the surface. The divergence signature at this time is weak and will only take 1-3 min to reach the surface. Of the 38 microbursts listed in Table 2, only three showed a distinctive single Doppler divergence signature above the 0.0° elevation angle prior to the initial divergence at 0.0°. This does not necessarily mean a multiple Doppler analysis would not have shown a weak mid-air divergence, only that it is difficult to detect from a

[3]The magnitude of the shear over ∿3 km is the most critical to aircraft performance.

FAA WJH Technical Center
00092761

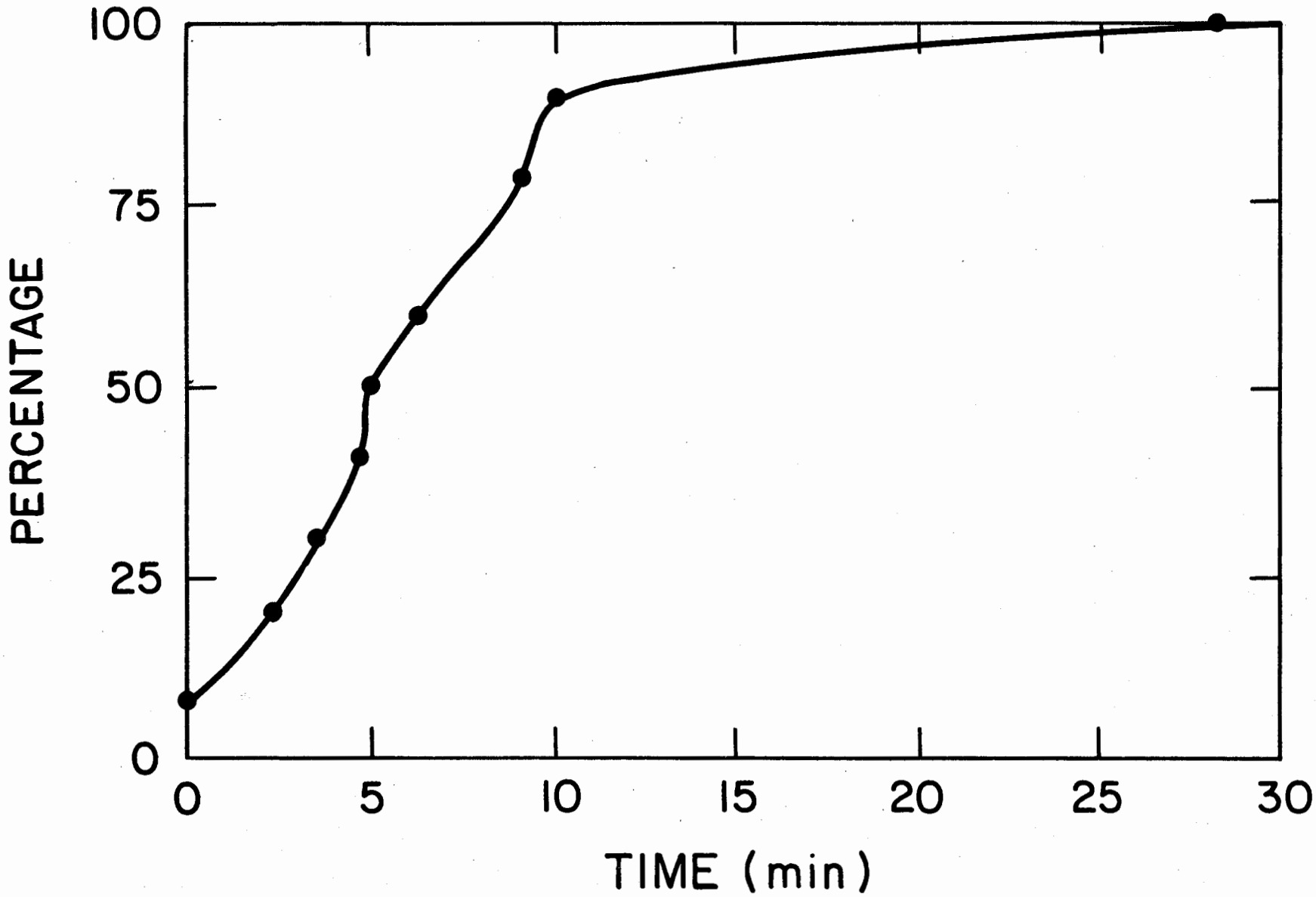

Figure 6. Percent of microbursts reaching maximum velocity differential as a function of the time from initial divergence.

Table 1. Asymmetry of low-altitude wind shear for 13 microbursts at various lengths.

			MAX. SHEAR $\frac{\Delta V}{\Delta R} \times 10^{-3}\ s^{-1}$					ASYMMETRY $\frac{\Delta V\ MIN}{\Delta V\ MAX}$				
			ΔR (km)					ΔR (km)				
Date	Time (MDT)	Case	0.6	1.0	2.0	3.0	4.0	0.6	1.0	2.0	3.0	4.0
05 August	1846	B3	28	24	15	9	--	.35	.28	.33	.26	--
14 July	1444	A	23	20	16	11	9	.50	.45	.48	.31	.39
05 August	1831	B1	20	13	9	6	--	.58	.43	.59	.35	--
13 July	1506	A1	18	15	12	9	6	.44	.33	.39	.41	.26
30 June	1829	A2	17	13	9	8	6	.71	.77	.66	.50	.41
14 July	1452	C1	15	12	8	8	5	.45	.35	.38	.34	.46
23 May	1422	A2	15	11	8	6	--	.45	.33	.47	.30	--
05 August	1831	B2	15	10	8	6	4	.22	.40	.40	.47	.48
05 August	1846	B4	13	14	5	2	--	.38	.21	.33	.19	--
05 August	1836	C	13	11	8	6	4	.38	.18	.18	.16	.34
08 July	1341	B	12	10	7	5	5	.50	.60	.53	.49	--
13 July	1506	A2	12	9	8	6	4	.67	.78	.53	.35	.23
14 July	1648	D	8	11	6	5	4	.60	.51	.67	.70	.51
AVERAGE			16.1	13.3	9.2	6.7	5.2	.48	.43	.46	.37	.39

Table 2. Time and space scales of microburst velocity differentials (ΔV_r) from the time of initial Doppler-observed, low-level divergence to maximum ΔV_r. The maximum reflectivity at 500 m within each microburst cell is also given.

Case	ΔV_r(m/s) Initial	ΔV_r(m/s) Maximum	ΔR(km) Initial	ΔR(km) Maximum	ΔT (Min)	dBZ_e (~500 m)
22 Jun A1	4	18	1.0	2.4	15.5	50
22 Jun A2	8	16	2.1	2.3	9	60
22 Jun B	16	22	2.2	4.2	7	60
23 Jun A	6	20	1.8	4.8	9.5	55
26 Jun A	18	18	1.5	1.5	0	25
26 Jun B	10	20	2.8	2.7	3	35
29 Jun C	12	29	1.3	2.5	5	20
29 Jun G	10	24	1.7	3.3	6	30
30 Jun A2	8	33	1.5	3.6	28	45
8 Jul B	14	24	2.8	3.7	6.5	30
8 Jul C	14	20	1.7	2.2	2	10
13 Jul A	18	22	2.5	2.8	2.5	45
14 Jul B	13	33	1.7	3.8	5	10
14 Jul C1	6	22	1.7	2.4	5	25
14 Jul C2	12	28	1.5	3.3	8	25
14 Jul D	10	27	2.0	3.3	5	50
15 Jul B	12	27	1.7	2.9	7	40
15 Jul E	12	20	1.8	4.3	4	40
15 Jul F	6	33	1.0	2.1	10	15
20 Jul A1	12	22	1.3	3.8	9	35
20 Jul A2	12	24	1.7	2.2	7	25
20 Jul B1	10	22	1.7	3.3	5	45
21 Jul B	22	26	3.1	3.8	2.5	55
28 Jul A1	12	12	2.2	2.0	0	50
3 Aug A	8	12	2.2	2.8	5	50
3 Aug C	12	16	2.7	6.0	5	25
5 Aug A	12	30	1.9	6.2	5	60
5 Aug B1	12	24	2.0	2.0	7.5	65
5 Aug B2	14	24	3.3	3.8	10	70
5 Aug B3	14	32	1.3	2.5	10	75
5 Aug B4	10	20	1.3	1.7	5	65
5 Aug C	6	26	1.1	2.6	8	70
6 Aug A1	6	22	2.0	2.4	8.5	70
6 Aug A2	22	26	1.4	2.1	2.5	65
6 Aug A3	10	16	1.4	1.5	2.5	55
6 Aug A4	37	37	2.4	2.4	0	50
6 Aug A5	14	26	1.0	1.7	3.5	50
12 Aug A	8	28	1.4	6.7	9.5	65
Average	12	24	1.8	3.1	6.4	45

single Doppler radar. The average initial surface velocity differential of 12 m s^{-1} in 1.8 km is similar to the lower boundary of an aviation hazard threshold suggested by the numerical simulation work of McCarthy and Norviel (1982). Thus, a successful aircraft penetration of a microburst should not be considered a nonhazardous case since in only a few minutes it may reach a dangerous magnitude. As soon as a microburst signature appears, whether aloft or at the surface, a warning should be issued, even if below hazard limit, since hazardous conditions may exist within 5 min. This would generate a number of false alarms since weak divergences are often observed that do not strengthen; this is a key point to be considered when developing detection and forecasting algorithms.

Microburst formation and driving forces are not yet understood; however, observational evidence suggests some common characteristics. For example, soundings for days when dry microbursts occurred were characterized by a moist layer around 500 mb with very dry adiabatic conditions below (Brown et al., 1982 and Caracena et al., 1983). However, this can only be used as a general indicator that dry microbursts may occur and specific information on time or location is not known. No information is yet known about necessary atmospheric conditions for other types of microbursts. Because microbursts tend to occur in families,[4] the detection of one should increase alertness levels for other occurrences. Again specific forecasts are not possible. We have noted several precursor signatures with individual radar echoes, such as rotation, strong convergence aloft, echo weak notch, and descending precipitation cores. Further examination of these potential signatures is just beginning. It remains to be established if reliable microburst precursors will be found, or whether their detection can be automated. If established, this would impact scanning requirements since observations would likely be required at heights far greater than those needed to scan along flight paths.

d. Summary of Microburst Structure and Evolution

We were impressed with the similarity between Doppler-derived microburst windfields here and flow structures proposed by Fujita and Wakimoto (1983) in their Fig. 4. Our Fig. 7 is a schematic representation of the evolution and flow within an average microburst as evidenced by the data in this paper. At T-5 min, where T is the time of initial divergence at the surface, the downdraft is above 2 km. There is negligible divergence and the downdraft is associated with a maximum rainfall rate core. At T-2 min, the downdraft is below 1 km and has begun to diverge horizontally. Horizontal roll vortices may be present on the edges of the outflow. At T, the downdraft speed has increased to about 10 m/s, the diameter is 1 km, the divergent outflow is <1 km deep and the maximum differential velocity is 12 m/s over a distance of 1.8 km. By T+5 min, the divergent outflow has spread horizontally and the maximum differential has increased to 24 m/s over a distance of 3.1 km. The depth of the divergent flow is less than 1 km and the downdraft speed has reached a maximum of about 12 m/s. At

---

[4]Of the 71 microbursts examined, 70% of them occurred on days when three or more were observed on the same day.

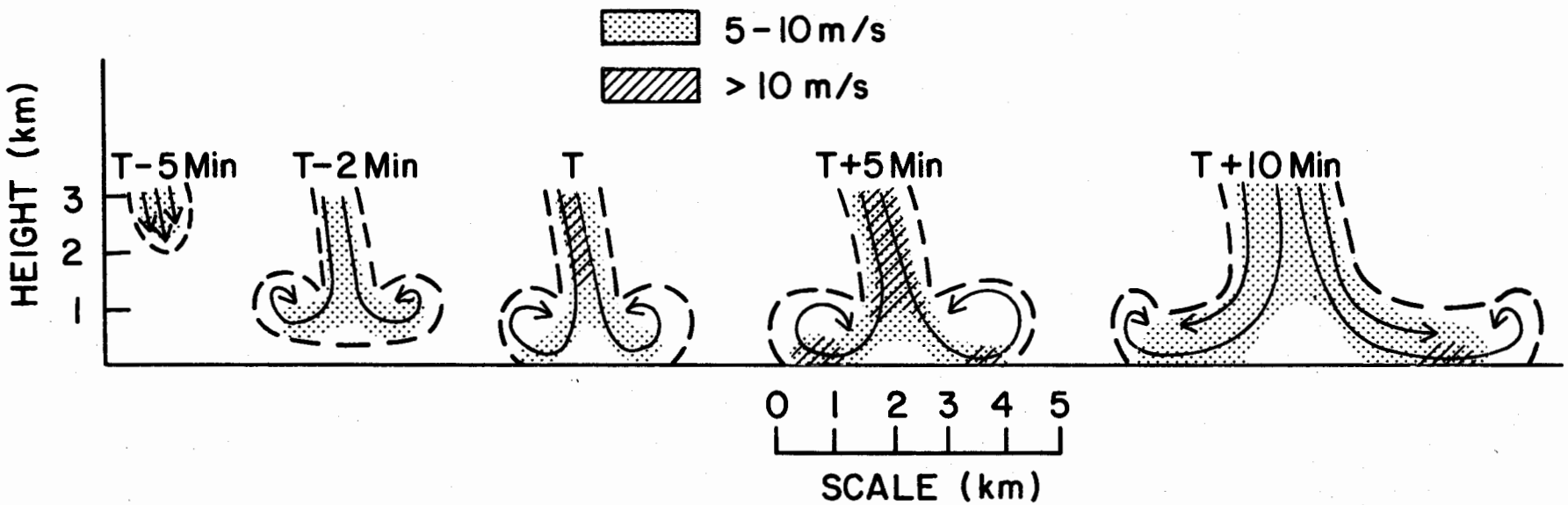

Figure 7. Vertical cross section of the evolution of the microburst wind field based on a summary of data in Section 3. T is the time of initial divergence at the surface. The shading refers to the vector wind speeds.

T+10 min, the downdraft has widened to 2-3 km but the speeds have decreased. The horizontal flow has weakened and spread to 6-8 km. After T+10 min, the flow frequently becomes weak and disorganized. On other occasions it continues to grow in horizontal extent with a similar pattern but with reduced speeds. In some instances, new microbursts will suddenly appear imbedded within the larger scale divergent flow. As the slope of the downdraft becomes more tilted with respect to vertical, it is expected that the leading edge outflow will be increasingly stronger than the trailing edge. Figure 7 represents the average JAWS microburst regarding evolution of the scale and magnitude of the outflow. From Table 2, no significant correlation is seen to exist between these parameters. The upper-level structure in Fig. 7 was heavily based on Fig. 3; however, vertical cross sections prepared for three additional microbursts after contact with the ground show similar features. The representativeness of the mid-air diverging flow at T-2 min is not known. Single Doppler analysis suggests it is frequently nonexistant or quite weak.

4. PROPOSED DOPPLER DEPLOYMENTS

Flight safety would be improved if detailed, rapidly updated wind information were available along the flight paths and if it were appropriately utilized. The location of microbursts and gust fronts in the terminal vicinity that are not yet affecting flight paths is needed as are forecasts of significant wind changes along flight paths. Numerical model and flight simulator tests (McCarthy and Norviel, 1982; Frost et al., 1983; and Fujita, 1983) suggest that the headwind-tailwind component is most critical to aircraft performance and thus is the most important to measure. We observed that hazardous shears at any one location are infrequent and that takeoffs and landings would probably need to be suspended for ∿10 min a few times a year. During JAWS there were 16 radar-observed microbursts within 10 km of Stapleton, representing only a small fraction of the convective storms observed within the same area. Thus, aircraft operations would need to be curtailed because of wind shear for a small percentage of the time that convective echoes are present. The task is to identify these occasions while keeping false alarms to a minimum. In this section, three possible Doppler systems for providing wind information in the terminal area will be discussed. They are: dual-Doppler, single-Doppler off-airport and single-Doppler on-airport. Only the detection and warning of wind shear in the vicinity of the airport by microwave Doppler radar is considered. The larger questions concerning the use of other sensors or if the radars should be used for detecting enroute hazards are beyond the scope of this paper.

From the results of Section 3, several general requirements can be placed on the radars for adequate detection of microburst winds. First, the radars must be able to measure reliable velocities in the lowest 1 km of the atmosphere whether in optically clear air, heavy rain, or hail. While it is desirable to observe the lowest 100 m, Fig. 4 shows observation of the lowest 100-500 m will usually provide a rough measure of the velocity differential below 100 m. From earth curvature considerations, the center of the beam for an elevation angle of 0° will be 100 m above the ground at 40 km. Because of blockage by intervening ground targets, the effective beam height is even higher, probably 200-400 m. Thus to adequately detect microbursts, the radar must be within ∿40 km of the airport

depending on the terrain and beam blockage. To ensure observation at a height of 100 m, the radar would need to be within ∿15 km. Second, the often small-scale nature of the microburst winds, i.e., 1-2 km between maximum approaching and receding velocities (Table 2) and the shallow depth of the outflow (<1 km) indicate that adequate resolution of the winds requires data resolution no greater than ∿250 m. Third, because of the short time scales involved, sampling at a rate of at least once per 2 min is desirable and data dissemination and assimilation must be within seconds. For example, less than 3 min elapses from the time the downdraft is above 1 km with no significant divergent signature until it reaches the surface, has significant divergence, and spreads horizontally. Fourth, it is impractical, if not impossible, for humans to interpret and disseminate the information in a timely manner; thus, the entire procedure must be automated.

a. Dual-Doppler

A dual-Doppler radar system could be deployed in which the radial wind components from each radar are combined, and the total wind field in the terminal area is specified up to a height of 1-2 km. This system is the only one proposed that could provide the three components of the wind along all flight paths; other systems would have more limited capabilities. Figure 8 shows a possible layout of radars with respect to an airport. Those labeled [a] depict a dual-Doppler array, with the radars located ∿14 km from the airport at ∿70° angles with respect to center field. The radars would need to scan a 90° sector to an elevation angle of ∿15° in 1° steps within 90 s. This could be accomplished with a pulse-repetition-frequency (PRF) of 1500 s^{-1} and a dwell time of 0.04 s, all quite feasible with today's technology. The stippled area in Fig. 8 shows the region where good dual Doppler winds can be acquired.

Great care would be required to ensure that the radars were observing close to the ground over the runways and that beam blockage was absent. To accomplish this, radars may require location on towers at tree-top height; however, finding suitable sites may be a significant problem. The primary disadvantage of this system is the initial high cost at each airport; also a high-speed data link is required to transmit the data to a central location where a dedicated computer would accomplish the dual-Doppler synthesis.

b. Single-Doppler, Off-Airport

Figure 8 also shows a possible off-airport location (labeled [b]). By siting the radar in line with a major runway, the wind component parallel to one flight path can be measured directly. For other runways, none of the three wind components could be measured directly, except perhaps a crosswind component if a runway were so located. The primary use of an off-airport location is to detect a microburst or gust front signature and locate it with respect to the flight paths. As shown above, the radar must be no further than 40 km and preferably within 20 km of the airport for microburst detection. There is no restriction on how close the radar could be located, except that both the azimuth and elevation scanning limits and ground clutter contamination would increase at closer ranges. The primary shortcoming with an off-airport site is the difficulty in estimating the true magnitude of microburst shear. In Section 3a, 92% of the microbursts

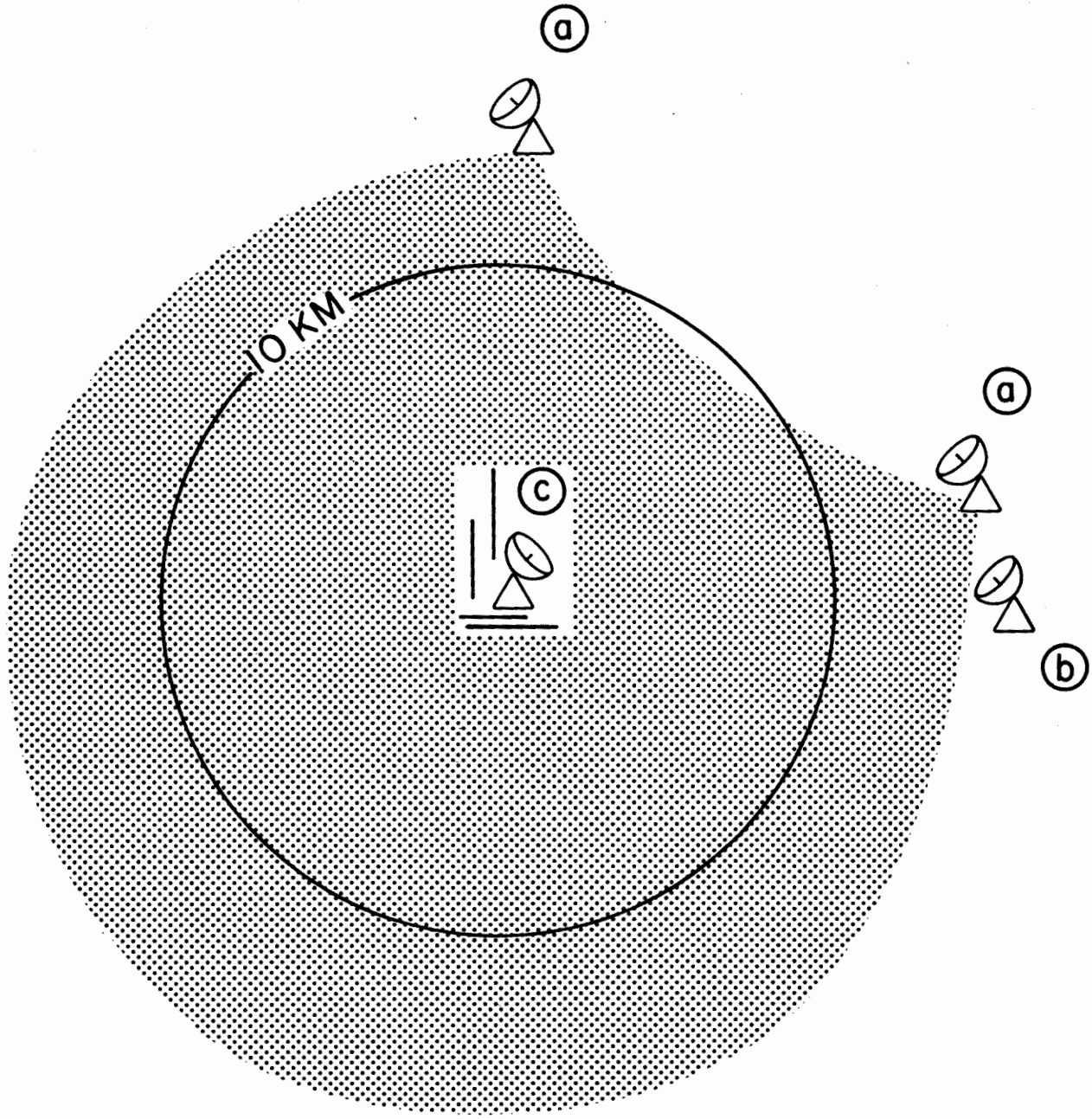

Figure 8. Locations of three proposed Doppler radar systems for detecting low-level wind shear near an airport. The airport is centered within the 10 km range ring. The radars labeled [a] represent a dual-Doppler system, the stippled area represents the area where accurate dual-Doppler winds can be obtained, [b] a single-Doppler off-airport system, and [c] a single-Doppler on-airport system.

observed by one radar were also observed by another radar with a different viewing angle. Because of asymmetry in the outflow (see Table 1), the shear magnitude could be greatly underestimated, unless independent means are found for determining the direction of the maximum shear axis.

To illustrate how an off-airport radar could significantly underestimate a hazard, the radial wind field for two hypothetical radars is derived for the microburst labeled B3, Aug 5 in Table 1. The actual near-surface (height 50-80 m) horizontal wind field is shown in Fig. 9a with a hypothetical 2.7 km long runway superimposed. Each hypothetical radar is located 13 km from the microburst center; the first is to the southeast along the axis of maximum shear and the other is to the northeast at a 90° angle to the maximum shear axis. The Doppler winds observed by the southeast radar, Fig. 9b, show a strong diverging couplet (16 m s^{-1} approaching and 12 m s^{-1} receding) along the runway. The northeast radar, Fig. 9c, shows little shear along the runway and only an 8 m s^{-1} differential across it. Thus the northeast radar greatly underestimates the actual hazard.

c. Single-Doppler, On-Airport

By locating a Doppler radar near the center of the airport (labeled [c] in Fig. 8), each flight path could be scanned and the important headwind-tailwind component directly measured, thus removing the ambiguity that exists with an off-airport location. Although the vertical wind component cannot be measured directly, a rough estimate can be made based on the strength of the divergence. The actual success in being able to look along each approach and departure path will depend on the organization of the runways at individual airports. Scanning in a 360° mode is necessary and limits the maximum scan height. With a PRF of 1500 s^{-1} and a dwell time of 0.04 s, a volume with elevation angles from 0° to 6° in $\sim$1° steps could be accomplished in 90 s, a sufficient period to obtain data along all flight paths. Also, reliable winds could be obtained within 100 m of the radar. As with an off-airport radar, this radar can be used to identify microburst locations using the divergence signature.

This radar may not be able to scan above the terminal to sufficient heights to detect clues of incipient microbursts. The importance of this deficiency is not known because reliable automated forecast signatures have not been established. If they are, judiciously directed elevation scans at constant azimuth (RHI) or 360° azimuth scans at high elevation angles might be useful. The possibility exists that an off-airport national network of Doppler radars (NEXRAD) may be responsible for detection of microburst precursors.

The dual Doppler option is the most desirable since it provides all three wind components within the terminal area. Siting of a single Doppler radar becomes primarily a choice between quantitative measurement of the headwind-tailwind component along at least some flight paths using an on-airport site versus using an off-airport site to scan high above the airport to possibly detect incipient microbursts. For the detection of wind shear hazards in the airport vicinity, both the on- and off-airport radars are equally likely to detect hazards based on shear signatures,assuming ground clutter is not a significant problem. The on-airport site has the advantage of being able to quantitatively measure the shear for at least

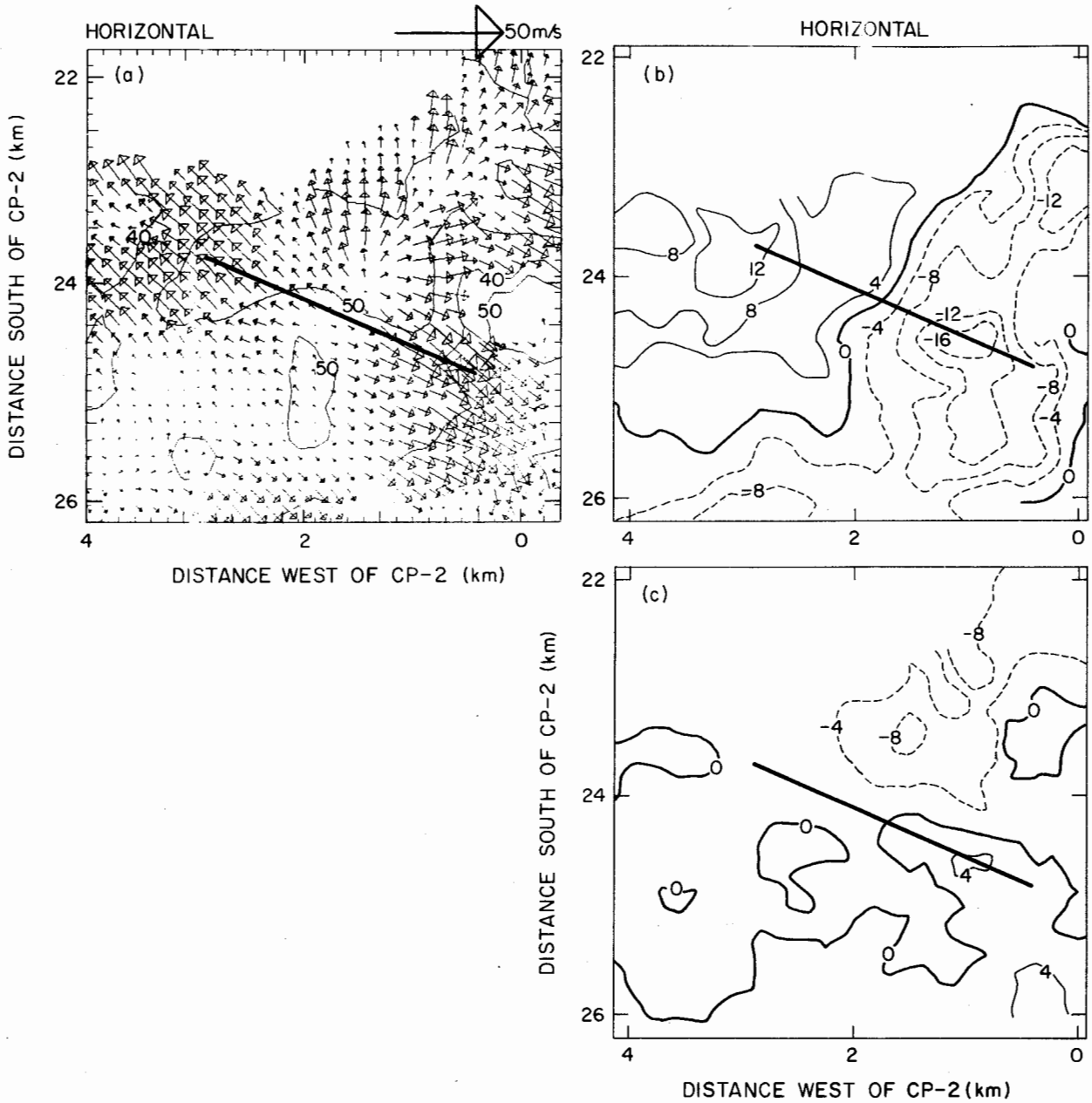

Figure 9. Simulation of the radial velocity field observed by two hypothetical off-airport radars viewing a microburst at 1846 MDT on 5 August 1982. (a) Actual horizontal windfield at a height of 50-80 m based on a dual-Doppler analysis. A hypothetical runway of 2.7 km is superimposed on the microburst. The contours represent radar reflectivity factors (dBZ_e). (b) Simulated Doppler radial winds for a radar located 13 km southeast of the microburst. (c) same as (b) except for a radar located 13 km northeast of the microburst.

some of the flight paths. As discussed earlier, reliable techniques for advance warning of microbursts based on precursor radar signatures have not been developed. If such techniques are developed and if they require scanning high above the airport, then the off-airport site would have an advantage.

d. Radar Characteristics

The major problem with the on-airport radar--and to a lesser extent the off-airport radars--is ground clutter. Another consideration is the need for sufficient sensitivity to detect clear air winds at low heights. Also, because the system needs to be largely automated, range and velocity ambiguities must be removed. Various signal coding and processing techniques have been proposed to alleviate this latter problem (Doviak and Strauch, 1980).

The use of shorter wavelengths should greatly improve ground clutter suppression. Given the same size antenna, for example, the beam width of a 3 cm radar will be 1/3 that of a 10 cm radar, thus sharply reducing main beam clutter.

Based on experience with the NCAR CP-2 radar which has a matched-beam 10 cm and 3 cm system, ground clutter at 10 cm is significantly stronger than at 3 cm. Rinehart and Tuttle (1983) have done an extensive comparison of the beam patterns and have shown the main beams are very similar. The side lobes, while different, cannot account for the major differences observed in the ground clutter returns. The first and strongest side lobes, 1.2° to 2.0° from the beam center, are higher for the 3 cm than the 10 cm. Since the comparisons are for low angles and many of the targets, particularly the mountains, are at elevated angles, most of the clutter is from the main lobe and first side lobe. Figure 10 is a comparison of 10 cm and 3 cm clutter patterns for an elevation angle of 0.5°. The radars are calibrated so they both measure the same reflectivity factors for light rain. It is apparent that the 10 cm clutter is more extensive. The N-S line of clutter to the west is from mountains. The well-defined, thin straight lines are power lines, and the remaining large clutter patches are low, rolling hills. Computer differencing of the Z_e images shows the 10 cm clutter ranges from 0-45 dB stronger than the 3 cm. The median difference is between 17 and 20 dB for elevation angles between 0° and 2.5°.

Simple backscattering theory considerations support the above findings. The backscattering cross section from precipitation targets (Rayleigh region) is inversely related to the fourth power of the radar wavelength (λ). The backscatter from ground clutter is not well established and is probably variable. If we assume scatter from clutter is in the optical region, the cross section is independent of wavelength. Skolnik (1980) shows in his Fig. 14.11 that this is essentially the case for many types of clutter. If we make this assumption, the ratio of the radar return from clutter to precipitation would be λ^4:1. This gives ratios of 10^4:1 and 3^4:1 for 10 cm and 3 cm, respectively. The ratio is 123 (21 dB) times higher for 10 cm, which is similar to what was observed by the 10 cm and 3 cm comparisons above.

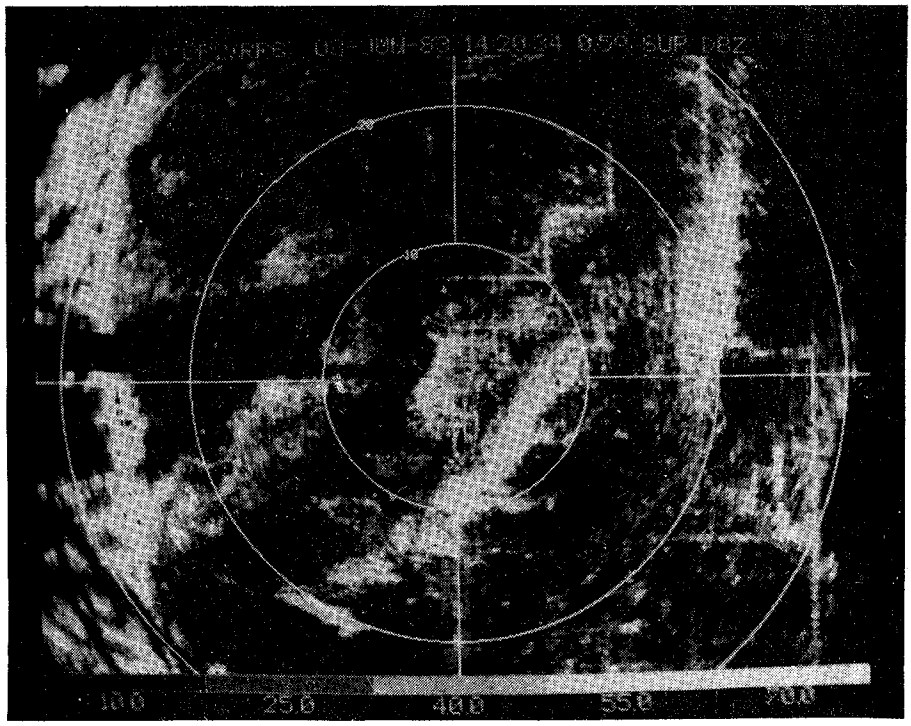

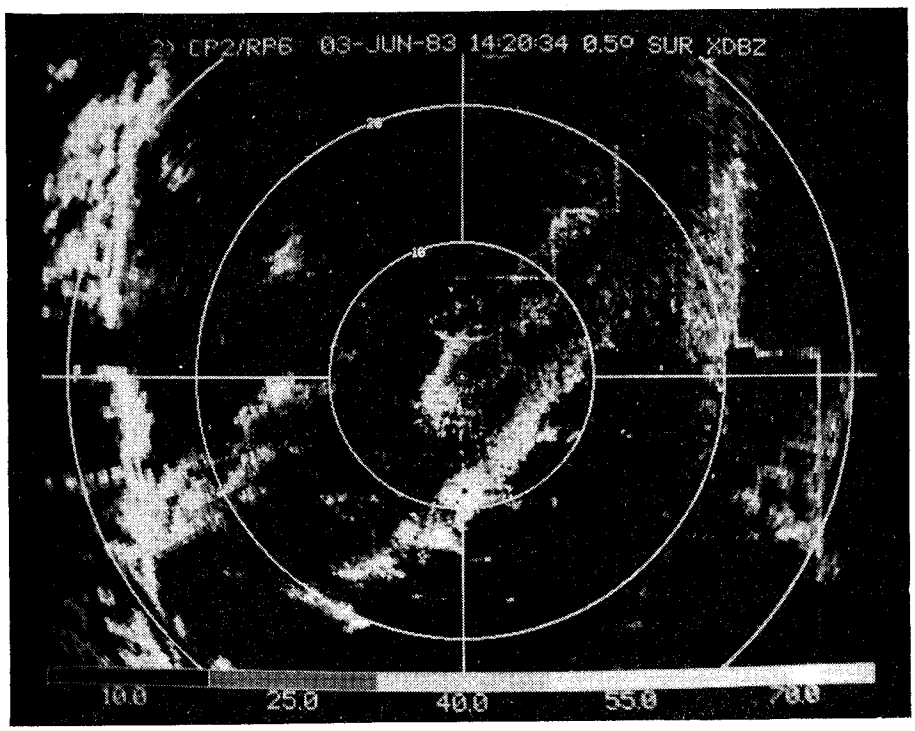

Figure 10. Comparison of ground clutter reflectivity patterns from collocated and matched beam 10 cm and 3 cm radars. Range marks are at 10 km intervals and the reflectivity scale is given by the bar at the bottom. The data are from the CP-2 radar scanning at an elevation angle of 0.5°.

Serious consideration should be given to newly available antenna technology for drastically reducing clutter contamination (Schrank, 1983). Phased array antennas with ultra-low sidelobes developed for the military are now commercially available. These antennas can routinely provide one-way sidelobes 40-50 dB down from the main beam. Antennas such as these would probably eliminate clutter as a serious impediment to microburst detection.

Electronic clutter cancellation techniques have also been proposed (Passarelli, 1983; Anderson, 1981; and Hamidi and Zrnic, 1981). Through improved antenna and electronic clutter cancellation, the likelihood exists that clutter can be reduced at least 40 dB from that of today's research radars.

Attenuation at 3 cm, and to a lesser extent at 5 cm, is a reason for often favoring 10 cm for weather radars. However, for airport windshear applications, attenuation is less significant because the maximum observing range is only 10-30 km and quantitative reflectivity measurements are not of primary importance. Also, provided the signal is not almost entirely attenuated, accurate Doppler velocities are possible. Utilizing attenuation information summarized by Battan (1973), 3 cm rainfall rates of $\sim$100 mm/h over a depth of 10 km would cause roughly 50 dB of attenuation. At 5 cm, it would be unlikely that rain rates of sufficient intensity would occur to produce velocity blind regions in the terminal area. However, Wilson (1978) has shown that 5 cm attenuations as large as 40 dB can occur in 10 km deep regions of large wet hail.

Attenuation may be a frequent enough problem that use of an off-airport 3 cm radar would be unwise. A 3 cm on the airport would rarely be attenuated sufficiently that velocities in the immediate terminal area (5 km radius) could not be observed. In all probability, the airport would already have been closed by hailfall and/or heavy rain. Attenuation problems for a 5 cm radar should be minimal, particularly if located on the airport.

Field experience with the NCAR 5 cm and 10 cm radars indicates that velocities in the clear air boundary layer are routinely observed during the convective season. However, similar experience with 3 cm is limited. While we have not conducted any definitive studies to determine the nature of scatters in the clear air, we believe that particulate scattering dominates over refractive inhomogeneities. For example, the observation in Section 2 on the typical clear air observation range of the 10 cm and 5 cm radars together with their minimum detectable signal suggests the scattering is by particulates, possibly insects. If this is so, then clear air detection with similarly sensitive 3 cm radars should be even better. However, if the primary scattering is non-particulates, this would not be true.

An off-airport site requires clear air detection to greater ranges, less attenuation, and less ground clutter suppression; this favors a 10 cm or 5 cm radar. On the other hand, an airport site can tolerate more attenuation and a shorter range for clear air detection, but requires a greater need for clutter suppression; this favors 3 cm or 5 cm. Tests will be required with various wavelength radars between 10 cm and 3 cm to determine

if ground clutter can be reduced to acceptable levels while maintaining full clear air detection.

5. CONCLUSIONS AND RECOMMENDATIONS

Data obtained during the JAWS Project were used to describe the temporal and spatial structure of wind within microbursts. These are summarized in Fig. 7 and Section 3c. This information is then used to discuss Doppler radar characteristics and siting and scanning strategies for warning the airport area of hazardous low-altitude wind shear; other weather hazards are not considered. Ground-based microwave Doppler radar is the only wind shear detection system considered in this paper. This does not mean other systems may not be equally or more effective. The following conclusions about the nature of microbursts impact the design of a Doppler radar system.

a) Microbursts are common, at least in Denver, and produce wind shears potentially lethal to aircraft. The average headwind-tailwind differences were 22 m s^{-1} with a maximum of 48 m s^{-1}.

b) They occur in a wide variety of convective storms that have effective reflectivity factors ranging from 10 to 75 dBZ_e. For many cases little or no rain actually reaches the ground even though microbursts were detected.

c) The surface divergence center is located in close proximity to a high reflectivity core; however, there are many cores that do not produce microbursts.

d) The horizontal dimension of the downdraft is roughly 1 km, and the horizontal extent of the outburst flow is 1-6 km.

e) The depth of the diverging flow is <1 km and the maximum horizontal wind shear is roughly around 75 m AGL, and decreases gradually above and below.

f) From the time diverging outflow first appears at the surface, 53% of the microbursts reach their maximum differential velocity within 5 min and 95% within 10 min. On some occasions they dissipate within 5-10 min, while on others they grow into large-scale events lasting 30-60 min.

g) The differential velocity, on the average, increases from 12 m s^{-1} to 24 m s^{-1} in the first 5-10 min.

h) The strength of the outflow is frequently asymmetric. On the average, the wind shear along the maximum shear axis through the microburst center is over twice that along the minimum shear axis. In the more extreme cases, it was 5-6 times greater.

i) Reliable forecast techniques have yet to be developed. General area-wide alerts for dry-type microbursts can be made based on vertical moisture and temperature profiles. Also for both wet and dry types the occurrence of one microburst increases the likelihood that others

will soon occur. Cell-specific, precursor clues have been observed. However, their reliability as forecast tools is uncertain. It was determined that a single Doppler radar usually did not detect significant divergence aloft prior to the surface microburst, thus making it an unreliable precursor.

Based on the above conclusions, the following recommendations are made concerning the radar system:

i) Radial velocities must be measured over a reflectivity factor range from -10 to 80 dBZ_e. This includes measurements in the optically clear air.

ii) The horizontal and vertical resolution of the data should not be greater than ~250 m. To obtain this resolution over the entire terminal area requires a half-power beam width of 1°. If antennas with ultra-low sidelobes are used, and if the radar is on the airport, somewhat larger beam widths may be tolerable.

iii) Automatic range and velocity unfolding is required.

iv) Ground clutter must be dramatically reduced from that of present research 10 cm and 5 cm radars.

v) Scan update rates must be about every 2 min. If reliable techniques are developed for accurately forecasting microburst time and strength, this might be relaxed.

vi) Techniques for identifying and disseminating wind shear information must be automated.

vii) A dual-Doppler system could provide all the needed wind information. While the initial cost may be larger than for a single Doppler system, it may prove more cost effective in the long run and it deserves serious consideration.

viii) It is not possible at this time to recommend an on- or off-airport site. The utility of an on-airport site is heavily dependent on greatly reducing ground clutter, and any advantage of an off-airport site depends on development of reliable automated techniques for advance warning of microbursts from Doppler signatures aloft.

Because of major uncertainties about ground clutter and clear air wind detection, it is not possible to specify a preferred wavelength. Before a system is purchased, it is strongly recommended that suitable experiments be conducted to answer three questions:

1. To what extent and for what price can close-in ground clutter be removed using new antenna technology and electronic signal processing? This is particularly important for 10 cm wavelengths since it is more susceptible to ground clutter than shorter wavelengths.

2. Can reliable boundary-layer clear air detection be obtained with 3 cm radars?

3. Can automated techniques be developed to reliably extract needed wind information from the Doppler data?

We feel confident that a Doppler radar system can be developed that could significantly reduce the number of wind shear accidents. However, its deployment does not automatically guarantee greater safety. Successful development of this system demands that the final product be delivered to the controllers and pilots in a concise, easily understood, reliable and timely form. This is more than a detail; in fact, we believe that the development of the final user product and its delivery system will require a greater commitment of time and people than development of the radar hardware.

6. ACKNOWLEDGMENTS

We would like to acknowledge Professor T. Fujita, of the University of Chicago, and Roger Wakimoto, of U.C.L.A., who were important members of the group that established and conducted the JAWS field program. We would also like to extend our appreciation to the following: the many NCAR Field Observing Facility technicians and engineers who made collection of the data possible; Wendy Schreiber for compiling data; Jay Miller, Richard Carbone and Mark Hjelmfelt, all of whom are at NCAR; and Edwin Kessler of NSSL for technical review of the paper; Phyllis O'Rourke and Carol Nicolaidis for editing the paper; Justin Kitsutaka for drafting the figures; and Margaret Miller and Shelley Zucker for typing the paper. JAWS is funded by NCAR, the National Science Foundation, the FAA through Interagency Agreement DTFA01-82-Y-10513, NASA through Interagency Agreement H59314B, and NOAA through a cooperative agreement with the Program for Regional Observing and Forecasting Services of NOAA's Environmental Research Laboratory.

7. REFERENCES

Anderson, J.R., 1981: Evaluating ground clutter filters for weather radars. Preprints, 20th Radar Meteor. Conf., Boston, MA, Amer. Meteor. Soc., 314-318.

Armijo, L., 1969: A theory for the determination of wind and precipitation velocities with Doppler radars. J. Atmos Sci., 26, 570-573.

Battan, L.J., 1973: Radar Observation of the Atmosphere. University of Chicago, IL, 324 pp.

Brown, J.M., K.R. Knupp, and F. Caracena, 1982: Destructive winds from shallow, high-based cumulonimbi. Preprints, 12th Conf. on Severe Local Storms, San Antonio, TX, Amer. Meteor. Soc., Boston, MA, 272-275.

Byers, H.R. and R.R. Braham, Jr., 1949: The Thunderstorm. Government Printing Office, Washington, D.C.

Caracena, F., J. McCarthy, and J. Flueck, 1983: Forecasting the likelihood of microbursts along the front range of Colorado. Preprints, 13th Conf. on Severe Local Storms, Tulsa, OK, 17-20 October 1983.

Carbone, R.E., 1981: Selected comments on multiple Doppler analysis. Preprints, 20th Radar Meteor. Conf., Boston, MA, Amer. Meteor. Soc., 490-494.

Charba, J. 1974: Application of gravity current model to analysis of squall-line gust front. Mon. Wea. Rev., 102, 140-156.

Cressman, G.P., 1959: An operational objective analysis systems. Mon. Wea. Rev., 87, 367-374.

Doviak, R.J., P.S. Ray, R.G. Strauch, and L.J. Miller, 1976: Error estimation in wind fields derived from dual-Doppler radar measurement. J. Appl. Meteor., 15, 868-878.

_____, and R.G. Strauch, 1980: The multiple Doppler radar workshop, November 1979--part III: single radar data acquisition. Edited by R.E. Carbone, Bull. Amer. Meteor. Soc., 61, 1169-1203.

Frost, W., H. Chang, J. McCarthy, and K. Elmore, 1983: Aircraft performance in a JAWS microburst. Preprints, 21st Radar Meteor. Conf., Edmonton, Alberta, Canada, Amer. Meteor. Soc., 630-637.

Frush, C., 1981: Dopper signal processing using IF limiting. Preprints, 20th Radar Meteor. Conf., Boston, MA, Amer. Meteor. Soc., 332-337.

Fujita, T.T., 1980: Downbursts and microbursts...an aviation hazard, Preprints 19th Conf. on Radar Meteor., Miami, FL, Amer. Meteor. Soc., 94-101.

_____, 1981: Tornadoes and downbursts in the context of generalized planetary scales. J. Atmos. Sci., 38, 1511-1534.

_____, and Roger M. Wakimoto, 1983: Microbursts in JAWS depicted by Doppler radars, PAM, and aerial photographs. Preprints, 21st Radar Conf., Edmonton, Alberta, Canada, Amer. Meteor. Soc., 638-645.

_____, 1983: Microburst windshear at New Orleans International Airport, Kenner, Louisiana on July 9, 1982. SMRP Res. Paper No. 199, University of Chicago, 39 pp.

Hamidi, S. and D.S. Zrnic, 1981: Considerations for the design of ground clutter cancelers and weather radars. Preprints, 20th Radar Meteor. Conf., Boston, MA, Amer. Meteor. Soc., 319-326.

Kessinger, C.J., P.S. Ray, and C.E. Hane, 1983: An Oklahoma squall line: A multiscale observational and numerical study. CIMMS Report and Contribution No. 34, Norman, Ok., 211 pp.

Mahapatra, P.R., R.J. Doviak and D.S. Zrnic, 1982: Radar detection of low-level windshear affecting aircraft terminal navigation. Proceedings of National Aerospace Meeting of Institute of Navigation, NASA-AMES, Mountain View, CA.

McCarthy, J., W. Frost, B. Terkel, R. Doviak, D. Camp, E. Blick, K. Elmore, 1980: An airport wind shear detection and warning system using Doppler radar. Preprints 19th Conf. on Radar Meteor., Miami, FL, Amer. Meteor. Soc., 135-142.

_____, J.W. Wilson, and T.T. Fujita, 1982: The Joint Airport Weather Studies (JAWS) Project. Bull. Amer. Meteor. Soc., 63, 15-22.

_____, and V. Norviel, 1982: Numerical and flight simulator test of the flight deterioration concept. NASA Contactor Report 35( ), NAS8-33458, Marshall Space Flight Center, AL, 35812, 31pp.

Miller, L.J. and R.G. Strauch, 1974: A dual Doppler radar method for the determination of wind velocities within precipitating weather systems. Remote Sensing Environment, 3, 219-235.

_____ and R.A. Kropfli, 1980: The multiple Doppler radar workshop, November 1979--Part II: experimental design and procedures. Bull. Amer. Meteor. Soc., 61, 1173-1177.

Mueller, C.K. and P.H. Hildebrand, 1983: The structure of a microburst as observed by ground-based and airborne Doppler radar. Preprints, 21st Radar Meteor. Conf., Edmonton, Canada, Amer. Meteor. Soc., 602-608.

NTSB, 1983: Aircraft Accident Report--Pan American World Airways, Clipper 759, N4737, Boeing 727-235, New Orleans International Airport, Kenner, Louisana, July 9, 1982. NTSB/AAR-83/82, National Transportation Safety Board, Washington, D.C., U.S. Government, 115 pp.

National Research Council, 1983: Low-altitude wind shear and its hazard to aviation. National Academy Press, Library of Congress Catalog Card Number 83-63100, 112 pp.

Oye, R. and R. Carbone, 1981: Interactive Doppler editing software. Preprints, 20th Radar Meteor. Conf., Boston, MA, Amer. Meteor. Soc., 683-687.

Passarelli, R.E., Jr., 1983: Parametric estimation of Doppler spectral moments: an alternative ground clutter rejection technique. J. Clim. & Appl. Meteor., 22, 850-857.

Ray, P.S., J.J. Stephens, and K.W. Johnson, 1979: Multiple-Doppler radar network design. J. Appl. Meteor., 18, 706-710.

_____, M. Gilet, and K.W. Johnson, 1980: The multiple Doppler radar workshop, November 1979--part IV: motion field synthesis and radar placement. Bull. Amer. Meteor. Soc., 61, 1184-1189.

_____, 1983: Personal communication. NSSL, Norman, OK.

Rinehart, R. and J. Tuttle, 1983: Dual wavelength processing: some effects of mismatched beam antenna patterns. Radio Sci., 18, Amer. Geoph. Union.

Schrank, H. E., 1983: Low sidelobe phased array antennas. Antenna and Propagation Society Newsletter, IEEE, Vol. 25, No. 2, 5-8.

Skolnik, M.I., 1980: Introduction to Radar Systems, McGraw-Hill, 581 pp.

Wakimoto, R.M., 1982: The life cycle of thunderstorm gust fronts as viewed with Doppler radar and rawinsonde data. Mon. Wea. Rev., 110, 1060-1082.

Wilson, J. W., 1978: Comparison of C- and S-band radar reflectivities in northeast Colorado hailstorms. Preprints, 18th Radar Meteor.Conf., Atlanta, GA, Amer. Meteor. Soc., 271-275.

_____, R. Carbone, and R. Serafin, 1980: Detection and display of windshear and turbulence. Preprints, 19th Radar Meteor. Conf., Miami, FL, Amer. Meteor. Soc., 174.

APPENDIX A

The values for the statistical uncertainty of the dual-Doppler derived winds presented in the text are based on the technique described in Doviak et al., (1976). This technique is recreated for a Cartesian coordinate system. For simplicity, the error variances are derived using only two Doppler radars. Inclusion of more than two radars (over determined system) results in a reduction of error variance over the strictly dual analysis (Kessinger et al., 1983).

Radar data are interpolated from radar space to Cartesian space using a distance-dependent (Cressman, 1959) weighting function, W_i,

$$W_i = \begin{cases} \dfrac{R^2 - r_i^2}{R^2 + r_i^2}, & r_i < R \\ 0, & r_i \geq R \end{cases},$$

where R is the length of the radius vector of influence used to describe either a spheroidal or ellipsoidal influence volume and r_i is the distance from the grid point to the observation. Data on or outside of the defined influence volume are not used in the interpolation. The length of the radius vector is generally equal to the horizontal and/or vertical grid spacing.

The weighting function is applied to the data within the influence volume to obtain the weighted-average grid point value, S,

$$S = \sum_{i=1}^{N} (W_i S_i) / \sum_{i=1}^{N} W_i ,$$

where the S_i are those data within the influence volume, totaling N in number. Radar data are interpolated to Cartesian space prior to the synthesis for the horizontal and vertical wind components.

The equations to derive the three dimensional wind field from two Doppler radial velocity estimates (Armijo, 1969) are:

$$(x-x_1)u + (y-y_1)v + (z-z_1)W = R_1 V_1 \qquad \text{(A1)}$$

$$(x-x_2)u + (y-y_2)v + (z-z_1)W = R_2 V_2 .$$

The quantities in parentheses indicate the x, y or z distances from the grid point to the radar (subscript 1 for radar 1 and 2 for radar 2) and R_1 and R_2 are the ranges from the two radars to the grid point. Radial velocity estimates from each radar are given by V_1 and V_2, the east and north wind components are u and v, respectively, and W is the sum of the vertical velocity (w) and the hydrometeor fallspeed (V_t) that is derived from radar reflectivity.

Using A1, the equations for the horizontal wind components are:

$$u = \frac{(y-y_2)R_1V_1 - (y-y_1)R_2V_2 + [(y-y_1)(z-z_2)-(y-y_2)(z-z_1)]\,W}{[(x-x_1)(y-y_2) - (x-x_2)(y-y_1)]}$$

$$v = \frac{(x-x_2)R_1V_1 - (x-x_1)R_2V_2 + [(x-x_1)(z-z_2)-(x-x_2)(z-z_1)]\,W}{[(x-x_2)(y-y_1) - (x-x_1)(y-y_2)]} \quad \text{(A2)}$$

From Eqs. A2 and the anelastic form of the equation of continuity,

$$\frac{\partial u}{\partial x} + \frac{\partial v}{\partial y} + \frac{\partial w}{\partial z} - \kappa w = 0, \quad \text{(A3)}$$

the vertical velocity is derived where κ is the logarithmic rate of change of density in the vertical. Integration proceeds upward from a boundary condition that w is exactly zero and using a staggered grid in the vertical. An iterative solution method is used to obtain the final u, v, and w estimates. The equation for w is:

$$w_{k+1/2} = \left(\frac{\left(\frac{1}{\Delta z} + \frac{\kappa}{2}\right)}{\left(\frac{1}{\Delta z} - \frac{\kappa}{2}\right)}\right) w_{k-1/2} - \left(2\Delta x\left(\frac{1}{\Delta z} - \frac{\kappa}{2}\right)\right)^{-1}\left(u_{i+1} - u_{i-1}\right)_k - \left(2\Delta y\left(\frac{1}{\Delta z} - \frac{\kappa}{2}\right)\right)^{-1}\left(v_{j+1} - v_{j-1}\right)_k . \quad \text{(A4)}$$

The indices i, j, and k represent the x, y, and z indices, respectively. Derivatives are approximated using a centered finite difference form and the integral is approximated by the trapezoidal rule.

Using Eqs. A2, the horizontal statistical errors are found by taking the variance of the velocity components. The variances are:

$$\mathrm{var}\,[u_k] \equiv \sigma_u^2 =$$

$$\frac{(y-y_2)^2 R_1^2 \sigma_1^2 + (y-y_1)^2 R_2^2 \sigma_2^2 + [(y-y_1)(z-z_2)-(y-y_2)(z-z_1)]^2 \sigma_{W_k}^2}{[(x-x_1)(y-y_2) - (x-x_2)(y-y_1)]^2}$$

$$+ \mathrm{cov}(u,w), \tag{A5}$$

$$\mathrm{var}\,[v_k] \equiv \sigma_v^2 =$$

$$\frac{(x-x_2)^2 R_1^2 \sigma_1^2 + (x-x_1)^2 R_2^2 \sigma_2^2 + [(x-x_1)(z-z_2)-(x-x_2)(z-z_1)]^2 \sigma_{W_k}^2}{[(x-x_2)(y-y_1) - (x-x_1)(y-y_2)]^2} .$$

$$+ \mathrm{cov}(v,w)$$

where σ_1^2 and σ_2^2 are the variances of the radial velocity estimates from radar 1 and radar 2 and

$$\sigma_{W_k}^2 = \left[\sigma_w^2 + \sigma_{V_{\underline{t}}}^2\right]_k .$$

The terms cov(u,w) and cov(v,w) represent the contribution of the covariance between the error in u and w and the error in v and w, respectively, and are caused by the iterative solution method used to determine the three wind components. These terms can be shown to be smaller than the contribution due to σ_w^2 (Ray, 1982) for this analysis and are neglected. The covariance between u and v is neglected due to its small size.

To solve for the vertical velocity variance, the same procedures are used as in the solution for the vertical velocity, i.e., upward integration of the anelastic equation of continuity from a specified boundary condition of w equals zero. Again, a staggered grid is used. The vertical velocity variance is:

$$\mathrm{var}\,[w_k] \equiv \sigma_w^2 =$$

$$1/2\left(1 + \left[\frac{\left(\frac{1}{\Delta z} + \frac{\kappa}{2}\right)}{\left(\frac{1}{\Delta z} - \frac{\kappa}{2}\right)}\right]^2\right) \mathrm{var}\left[w_{k-1/2}\right] + \left(2\Delta x\left(\frac{1}{\Delta z} - \frac{\kappa}{2}\right)\right)^{-2} \mathrm{var}\left[u_k\right] + \left(2\Delta y\left(\frac{1}{\Delta z} - \frac{\kappa}{2}\right)\right)^{-2} \mathrm{var}\left[v_k\right] . \tag{A6}$$

Using Eqs. A5 and A6, the relative contribution to the statistical error of each of the three wind components is evaluated. Assumptions made include: A value of unity for the radial velocity variance from both radars and a value of unity for the terminal velocity variance. Summation of var $[u_k]$ and var $[v_k]$ leads to the horizontal (or divergence) error variance.

This technique has been programmed into the NCAR/FOF VAX 11/780. Using the JAWS radar locations, the statistical uncertainties are assessed at the storm position and the computed values are given in the text.

APPENDIX B

Radar data editing is a subjective process relying heavily on the analyst's experience and familiarity with the radars. Recently, this process has been greatly simplified and the accuracy substantially increased through the use of highly interactive software and versatile color displays. The editing system used here has been discussed by Oye and Carbone (1981). Editing functions included removal of data contaminated by ground clutter, side lobe echoes and "second trip" echoes; also, "folded" Doppler velocities were corrected. With the exception of ground clutter contamination, editing was straightforward with little difficulty.

A ground clutter map obtained during non-precipitation periods was used to facilitate the editing of clutter velocities. Because of significant time variability in the intensity of the clutter return, it is not sufficient to edit solely on the basis of a clutter map. However, by utilizing time and space continuity of the radial velocity fields on both horizontal and vertical surfaces from all three radars together with their individual clutter maps, it is usually quite easy to determine which zero velocities are clutter and which are weather. In areas where the "capturing effect" (discussed in Section 2) does not work, the contaminated velocities are not zero but only biased toward zero. These areas are generally easy to identify since they are in areas of low signal strength or where the clutter and weather are of similar signal strength.

Radial velocities identified as wrong in the raw data fields are deleted and no attempt is made to fill these missing data areas. In the wind synthesis process, if an individual grid point does not have data from at least two radars, no wind will be available for the grid point.